



University of
Southern Denmark

Rocket Stabilization System

Bachelor Project

Supervisor	Anders Stengaard Sørensen
Hand in date	2. June 2025
Institution	University of Southern Denmark
Study Program	Bachelor of Science in Robotics
Number of Pages	60

Harald Bay Baastrup	hneil22@student.sdu.dk	19-01-1999
Aksel Møller-Hansen	akmoe22@student.sdu.dk	24-07-2001
Sebastian Laugesen Piessenberger	sepie22@student.sdu.dk	07-08-2001

1 Abstract

This project presents the design and development of a stabilization system for a water rocket utilizing reaction wheels, laying the foundation for future systems to neutralize drones. The goal is to investigate the possibility of maintaining a vertical trajectory during the rocket's acceleration phase using a reaction wheel system, which regulates both roll and pitch axis.

The rocket, based on a 2 L soda bottle, is propelled by water and pressurized air. The rest of the rocket is modular and 3D-printed to allow rapid prototyping and replacement. The stabilization system includes a Raspberry Pi Pico W microcontroller, an IMU sensor, a microSD card, and a pair of ESCs powering BLDC motors.

To control the rocket, reaction wheels and motors are used to apply a torque to the rocket. Torque estimation is investigated using both theoretical calculations and load cell measurements, providing an estimated torque of 0.1246 Nm.

A PD controller is implemented to regulate the system based on angle feedback, where a complementary filter is used to combine accelerometer and gyroscope data from the IMU.

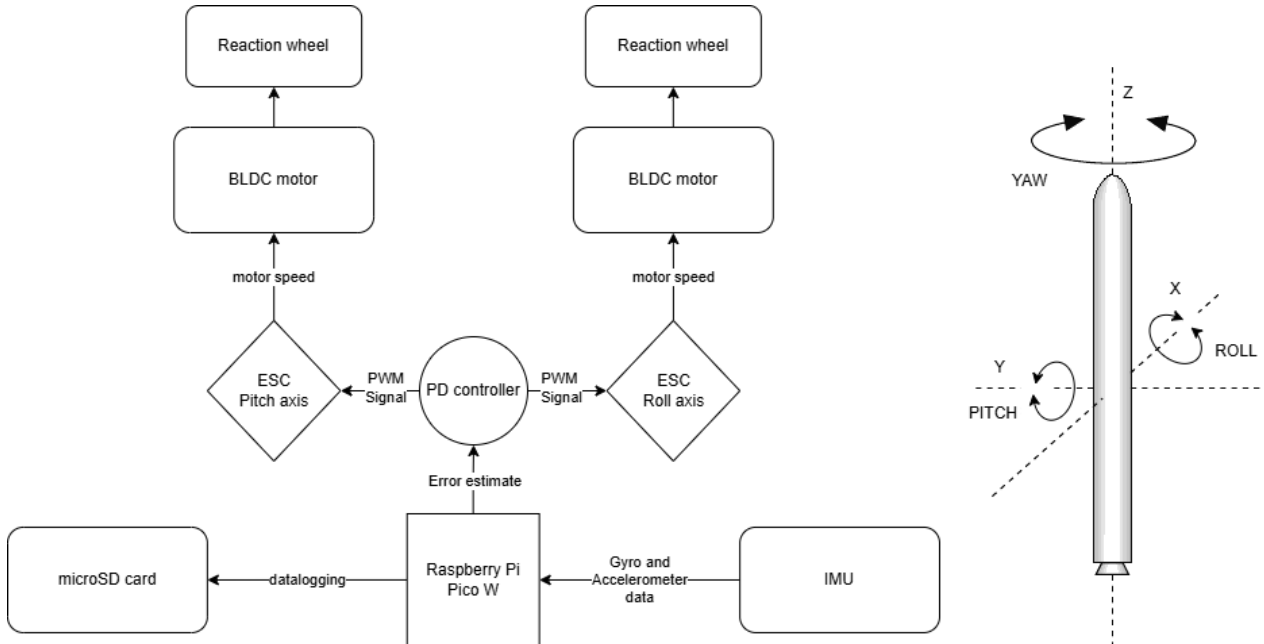


Figure 1: Stabilization System diagram and Rocket orientation representation.

Through testing the performance of the stabilization system is evaluated, but it is primarily

tested with a single BLDC motor controlling one axis due to motor defects. The results indicate that the reaction wheel is able to influence angular stabilization during acceleration, though further testing is required to conclude the indications to be facts.

Table of Contents

2 Introduction	5
3 Problem statement	5
3.1 Project aim	5
3.2 Project limitations	5
4 Rocket design	7
4.1 Intermediate body and nose cone	7
4.2 Reaction wheel	9
4.3 Mold interface for bottle	10
5 Microcontroller	12
5.1 Pico W	12
5.2 State Machine	12
5.3 PCB	14
6 BLDC Motor, ESC and Battery	15
6.1 BLDC motor	15
6.2 Electronic Speed Controller	15
6.3 Battery	17
7 Motor torque	18
7.1 Theoretical moment of inertia	18
7.2 Unsuccessful Attempt at Torque Estimation	19
7.3 Torque Estimation Using Load Cell	19
8 IMU	24
8.1 Accelerometer	24
8.2 Gyroscope	25
8.3 Complementary filter	25
9 Controller	27
9.1 PD Controller	27
10 Testing of Stabilization System	29

10.1 Rocket Launch system	29
10.2 Data Control Test	29
10.3 First Test of the Stabilization System	31
10.4 Second Test of Stabilization System	32
10.5 Third Test of Stabilization System	32
10.6 Fourth Test of Stabilization System	34
10.7 Fifth Test of Stabilization System	36
10.8 Sixth Test of Stabilization System	37
11 Discussion	38
11.1 RTOS	38
11.2 Launchpad changes	38
11.3 Force and Pressure Measurement	39
11.4 Fully Integrated Water Rocket Design	39
11.5 BLDC motor and ESC	39
11.6 Torque Estimation	40
11.7 Complementary Filter	40
11.8 IMU Evaluation	41
11.9 Controller Evaluation	41
11.10 Evaluation of the testing	41
12 Conclusion	43
13 Bibliography	45
14 Appendix	47
14.1 Rocket Design and Launch System	47
14.2 Videos	49
14.3 ESC Programming	51
14.4 Data Control Test Graphs	53
14.5 First Test Graphs	54
14.6 Third Test Graphs	56
14.7 Fourth Test Graphs	58
14.8 Fifth Test Graphs	59
14.9 Sixth Test Graphs	60

2 Introduction

The popularity and accessibility of drones have grown in recent years, making it challenging to regulate illegal drones that may broadcast paid or classified events. Firstly, drones need to be detected, targeted, then neutralized by a rocket with mid-flight trajectory control, vector thrusting, or other means of regulation. A rocket using rocket fuel as a propellant can be dangerous and have a negative effect on society, especially if people are close by.

This project explores the development of a rocket designed to neutralize drones, with the primary objective of creating a foundation for stabilization using reaction wheels during the acceleration phase. The rocket will be developed around a soda bottle using pressurized air and water as propellant, giving the opportunity to achieve a cheap and acceptable solution to neutralize drones.

3 Problem statement

This project utilizes reaction wheels, applying torque to adjust the trajectory of a water rocket. Additionally, the project includes initial testing of the reaction wheels' capabilities. This project is a sub-project for a complete system capable of pre-launch targeting, active stabilization during acceleration, and mid-flight trajectory adjustments, originally intended for drone neutralization.

3.1 Project aim

- Develop a rocket without fins using a 2L soda bottle.
- Develop a controller to regulate the rocket into a vertical trajectory.
- Testing the performance of the rocket during acceleration.

3.2 Project limitations

This project does not include pre-launch drone targeting and mid-flight trajectory adjustments. Furthermore, external factors such as wind speed, drag and ground unevenness are not accounted for in the project.

Additionally, internal variables such as the water level and air pressure within the bottle have a significant impact on the rocket. However, these are excluded from consideration, but the consequences will be discussed.

4 Rocket design

This project is based on a water rocket that uses compressed air and water as the propellant. A 2 L soda bottle is selected early in the design process due to its capacity and shape. Building on this foundation, the rocket follows a 3D printed modular design: including a nose cone, dedicated modules for the reaction wheel and battery, and a custom-made mold to interface with the bottle as seen in fig. 2.

4.1 Intermediate body and nose cone

The constraints of the design are set by the 2 L soda bottle and limiting the weight of the rocket.

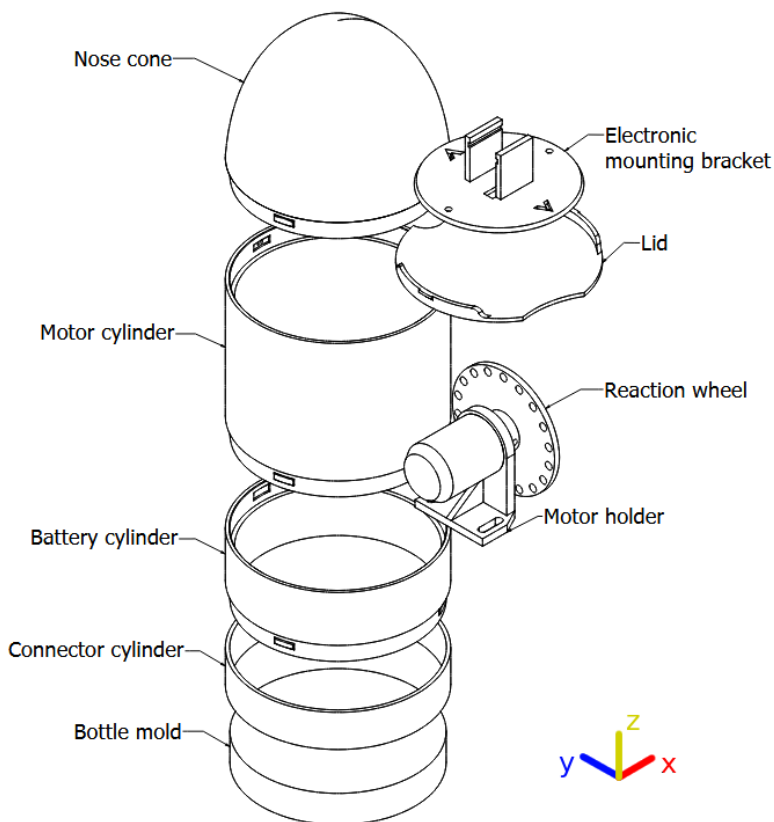


Figure 2: Rocket modules, with only one motor and battery cylinder

The rocket is made of different modules as seen in fig. 2 and appendix 14.1. The nose cone contains an IMU (Inertial Measurement Unit) and other electronics for controlling the rocket, all

connected by a custom PCB (Printed Circuit Board) as seen in section 5.

The IMU is placed in the slot on the electronic mounting bracket at the top of the nose cone. It defines the orientation as seen in fig. 2, with the Z-axis upwards. The placement of the IMU in the nose cone is used to maximize acceleration for the accelerometer.

The PCB is placed at the bottom of the electronic mounting bracket. To secure the IMU, PCB, and mounting bracket, the nose cone contains recessed nuts. With the nose cone placed above the motor cylinder, a lid is placed in between them, to protect the electronics from the rotating reaction wheel during flight and landing. The lid and the cylinders contain a wire slot for the power and signal wires from the ESC to the PCB in the nose to prevent entanglement with spinning reaction wheels.

The motor cylinder holds the assembled motor and reaction wheel. It is placed above the battery cylinder, which contains the battery and the ESC (Electronic Speed Controller) for the motor, which is introduced later in section 6.2.

The battery and motor cylinders form a single-axis reaction wheel system. To enable control of both the roll and pitch axis, an identical pair can be added, where the motor can be rotated 90 degrees, as shown in fig. 3.

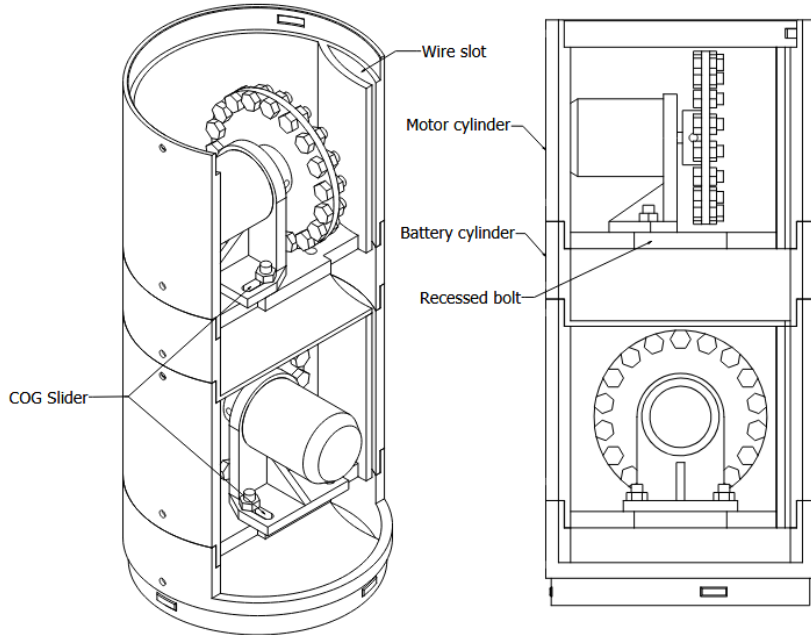


Figure 3: Motor placement for roll and pitch axis

The mounting holes for the motor holders are parallel to the IMU axes, minimizing force decomposition measured by the IMU. Furthermore, the mounting holes are enlarged on the bottom, concealing the bolt to avoid sharp edges in the battery cylinder. As a means to adjust the center of gravity, the motor holder can slide back and forth when the nuts and bolts are loosened, as seen in fig. 3.

To connect the segments together, a tab is placed on the outside of the modules, matching with an inverted tab on the inside depending on the placement of the segments as seen in the top and bottom of fig. 3. The tabs are placed with 70° shift from each other. This ensures the modules can be connected in different order, but always with the same orientation. Furthermore, an indent is added to make it visible from the outside which sides need to line up. Lastly, a hole is added to the nose cone in order to fit a red LED inside for the state machine blink indications, which is described in section 5.2.

4.2 Reaction wheel

The reaction wheels are fundamental in controlling the rocket as they provide the torque (τ) used for steering the rocket in the desired direction. A crucial part is the reaction wheels' ability to generate torque, where the moment of inertia and acceleration need to be sufficient to overcome the rocket's inertia. Torque is generated by a combination of angular acceleration and moment of inertia as seen in eq. (1).

$$\tau = I \cdot \alpha \quad (1)$$

Moment of inertia is given by eq. (2), where m_i is the mass of a point, and r_i is the point's distance from the rotation axis.

$$I = \sum m_i r_i^2 \quad (2)$$

To increase the moment of inertia, the radius of the wheel is dimensioned to fit within the motor cylinder. The primary mass of the reaction wheel is added in the circumference using nuts and bolts as weights. In practice, this is done by 3D printing the wheel with holes for nuts and bolts around the edge, as illustrated in fig. 4. To finetune the reaction wheel's inertia to the mo-

tor, longer bolts can be fitted together with more nuts to increase the inertia. However, the motor must still be able to accelerate the reaction wheel at a satisfactory acceleration level.

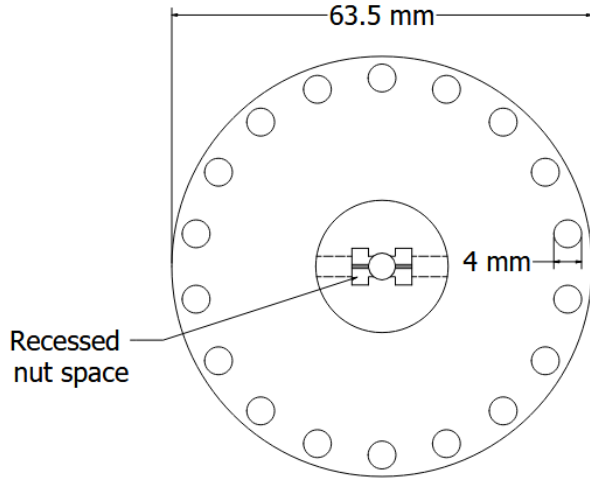


Figure 4: Reaction wheel design

To lock the reaction wheel to the motor axle, nuts can be recessed into the reaction wheel, as shown in fig. 4. This ensures a strong thread when the bolt is tightened against the axle. To reduce vibration, another set of nuts and bolts are mirrored to the opposite side.

4.3 Mold interface for bottle

To connect the rocket modules with a 2L soda bottle, a mold of the bottle's bottom geometry is created. With no available CAD model of the used soda bottle, a 3D scan of the bottle's bottom section is performed.

The scanning process is carried out by capturing multiple high-resolution images of the bottle from multiple angles, surrounding the entire bottle. For these images, flour is applied to the surface of the bottle, to capture the transparent plastic.

These images are then processed in the online service Kiri Engine [7], which generates the 3D mesh of the bottle shown in fig. 5a.

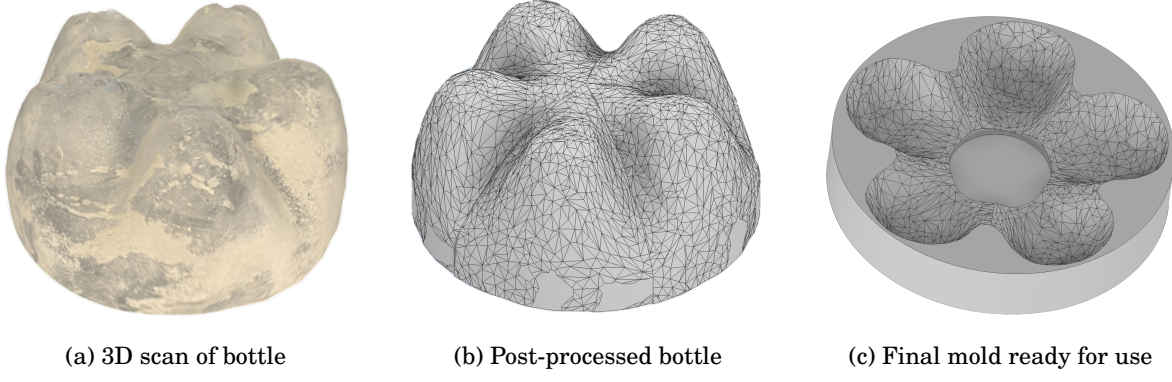


Figure 5: Creation of mold using 3D scan, post-processing in CAD, and final mold design.

The raw scan produced irregularities caused by surface reflections and uneven flour coverage during image capturing. As a result, post-processing CAD software [1] is required to refine the geometry.

Finally, the modified bottle scan is transformed into a cylindrical mold as seen in fig. 5c. This mold ensures a consistent and secure fit between the bottle and the custom modules.

5 Microcontroller

To operate, steer, and data log, the Raspberry Pi Pico W microcontroller is used. For the Pico W to know its orientation an IMU is used where the data from the IMU and the PWM to the ESCs, are logged on a microSD card. Since a launch consists of the same steps every time, a state machine are used for consistency. To further improve the setup a PCB is made to reduce troubleshooting.

5.1 Pico W

The Pico W is a microcontroller board based on the Raspberry Pi RP2040 microcontroller chip [10]. The board has a buck-boost converter to step down the voltage from 5.5 V to 3.3 V. This makes it possible to power it from an ESC with a BEC (Battery Eliminator Circuit). The 3.3 V from the Pico is used by the microSD card and the IMU.

To control an ESC, the Pico W needs to generate a PWM signal. When connecting external hardware, the GPIO pinout figure [10, p. 5] is used to determine which pins are usable. Two pins are used for the PWM signal, one for each motor. To log the data, a microSD card is used with a breakout board [14]. For simplicity a FatFs library [4], tailored to the Raspberry Pi Pico family is used. Before first use, the microSD card needs to be formatted to the FAT (File Allocation Table) protocol for compatibility. Besides pins for PWM, the Pico W communicates with the IMU over I^2C (Inter-Integrated Circuit), and with the microSD card via SPI (Serial Peripheral Interface).

Instead of a button to start the reaction wheel, a trigger wire between the Pico W and ground is used. To prevent false readings the Pico W uses an internal pull-up resistor. To visually see when the rocket is ready, a red LED is used.

5.2 State Machine

A state machine is developed to monitor and manage errors that may occur during a launch and flight. It also ensures the motors are activated, and the IMU is reset at the correct time.

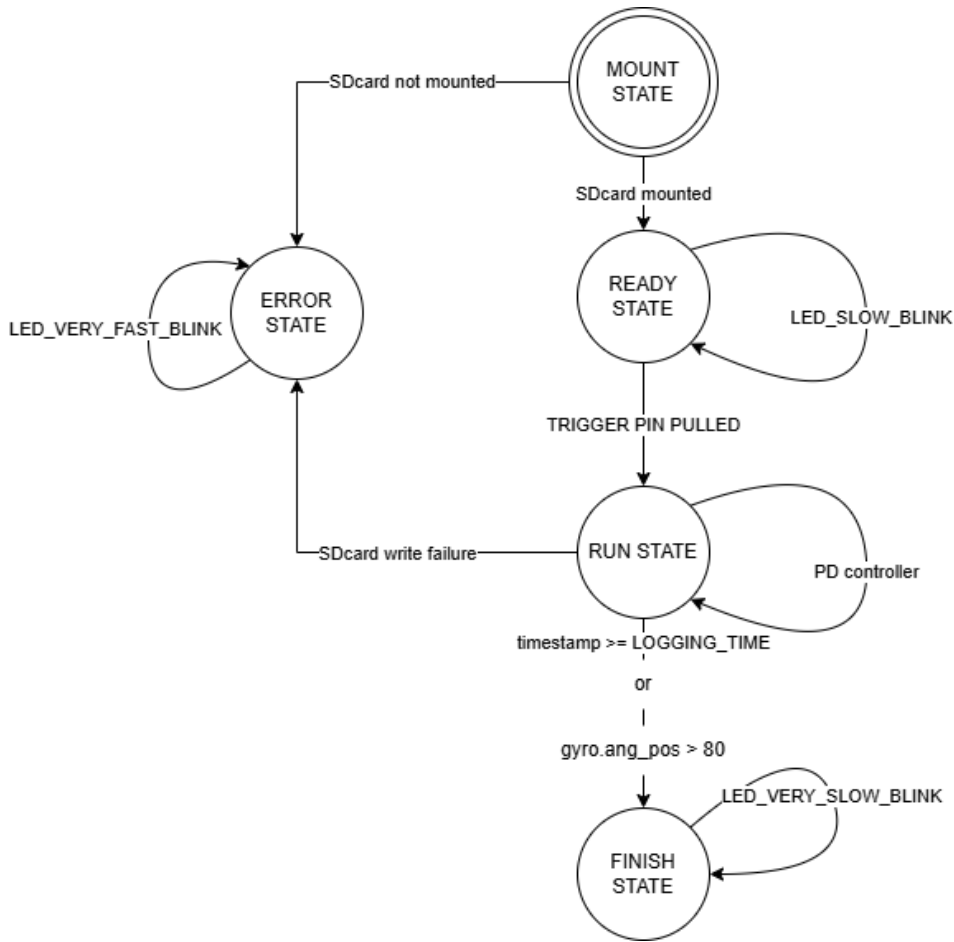


Figure 6: State Machine Diagram

As shown in fig. 6, the initial state is the MOUNT STATE, where the system checks whether the microSD card is properly mounted. If the microSD card is not mounted, the system transitions to the ERROR STATE, during which no further operations occur, and the LED blinks very fast to indicate a failure.

If the microSD card is successfully mounted, a .txt file for data logging is made before the state machine transitions to the READY STATE. In this state, the LED blinks slowly, indicating readiness, and the trigger pin can be activated to proceed to the RUN STATE.

In the RUN STATE, the motors are activated and the PD controller begins regulating the rocket, while data is written to the microSD card. If, during the RUN STATE, the microSD card becomes unmounted or write failure occurs, the system will transition to the ERROR STATE.

After a logging period of 30 seconds, or if the nose cone is detected to be sideways, the system transitions to the FINISH STATE. Here, the LED blinks very slowly and the system can be powered off without corrupting the data.

5.3 PCB

The rocket is exposed to high impact forces during crash landings. To minimize the risk of broken wires and simplify troubleshooting, a simple PCB has been made.

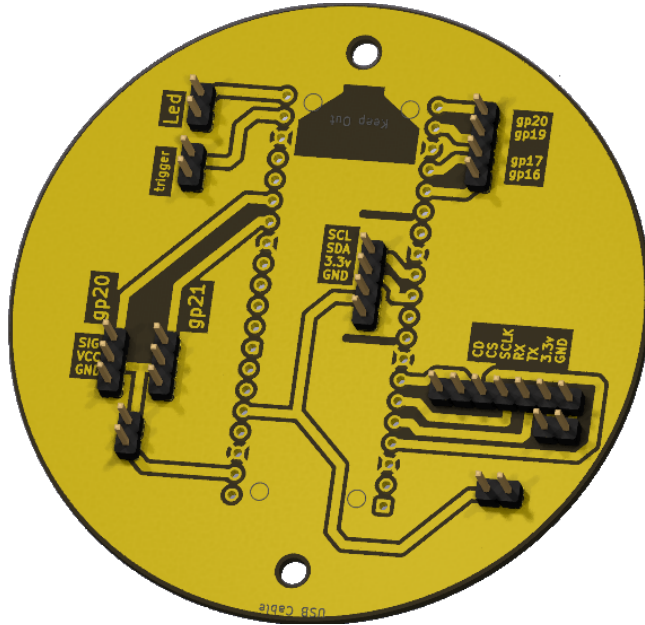


Figure 7: The holes fit the recessed nuts in the nose cone

The BEC power, 5 V and ground, from both ESCs are routed in parallel to pin headers on the PCB. In this configuration, inserting either ESC supplies power to the system. However, to ensure both ESCs are properly connected before powering on, a two-pin header is placed in series on the 5 V power line. This means the system will only boot when a jumper wire is inserted, acting as a manual power switch as seen in the bottom left corner of fig. 7. The 5 V is routed into the boost buck converter on the Pico W. Internally the Pico W needs 3.3 V, which it also outputs to the microSD card and the IMU. The data lines for the I^2C and SPI communication are routed to the relevant Pico W pins. The PCB also includes soldering pads for the red LED and trigger pin for the state machine.

6 BLDC Motor, ESC and Battery

In this project, BLDC (Brushless Direct Current) motors are provided for generating torque with the reaction wheels along the roll and pitch axes. To utilize the capabilities of the motors, a compatible pair of Electronic Speed Controllers (ESC) are chosen. Finally, a suitable battery is chosen to comply with the system's voltage and current requirements.

6.1 BLDC motor

The motor needs to be able to accelerate the reaction wheel to generate torque on the rocket. If the motor reaches its maximum RPM, it then loses the ability to compensate for rocket rotation in one direction. If a motor has a high maximum RPM, it has a larger interval to accelerate before saturation. To avoid saturation, the motor should be able to sustain acceleration over longer periods while having a large torque.

Due to time constraints, the BLDC motor used in this project is the EMAX GT2218/09 1100Kv [5].

The BLDC motor supports a maximum current of 24 A and is designed to operate with a 3-cell lithium polymer (LiPo) battery [5]. A fully charged 3-cell LiPo delivers 12.6 V [18].

The unloaded RPM of the motor can be calculated using its Kv rating, which specifies RPM per volt:

$$RPM = Kv \cdot V = 1100 \frac{\text{RPM}}{\text{V}} \cdot 12 \text{ V} = 13200 \text{ RPM} \quad (3)$$

As seen in eq. (3), this result of 13,200 RPM represents the theoretical maximum speed when the motor is spinning without the reaction wheel attached. In practice, the rotational speed is reduced when driving the inertia of the reaction wheels [15]. In the context of this project, a higher maximum speed is beneficial, as it provides a longer acceleration phase.

6.2 Electronic Speed Controller

To control the BLDC motor, a Reely Sky-Series 20 A ESC is selected[2]. Originally, the ESC is designed for RC aircraft use with slower accelerations, which differs from the desired rapid

accelerations, but this is addressed in section 6.2.3. Although being a 20 A ESC, the ESC supports burst current draw up to 25 A for short time intervals of 10 seconds [2], which meets the requirements of the BLDC motors.

This ESC is unidirectional, meaning it cannot reverse its direction of rotation during use, but only by swapping two wires to the motor [2]. This limitation poses challenges when balancing the rocket in both positive and negative directions of roll and pitch axis. To work around this, the system uses rapid acceleration and braking of the motor to generate torque in both directions, thereby enabling bidirectional stabilization despite the unidirectional rotational constraint.

Additionally, the ESC includes a built-in BEC, which is used to power the Pico W.

6.2.1 PWM Interpretation

The ESC used in this project operates using standard servo-style PWM signals, commonly used in hobbyist applications. This type of PWM control uses pulse widths to indicate throttle levels, rather than varying duty cycles as is typical for general-purpose PWM in embedded systems.

The ESC expects a signal with a 20 ms period (50 Hz), where a 1 ms pulse corresponds to 0% throttle and a 2 ms pulse corresponds to 100% throttle [9].

6.2.2 ESC Behavior

The ESC has a dead-zone or zero-throttle region from 0% to 10% throttle, corresponding to PWM pulse widths between 1.000 ms and 1.100 ms.

Once the 10% threshold is reached, the motor responds with audible beeps, as illustrated in the "Normal startup procedure" in appendix 14.3. These beeps signals that the motor is armed and capable of spinning. Once armed, the ESC requires a minimum of 20% threshold to initiate rotation but can still immediately respond to full throttle range. As long as the motor remains active, this startup procedure does not need to be repeated when reducing throttle back to 0%.

6.2.3 ESC Programming

When using the ESC for the first time, it defaults to standard settings which may not provide sufficient acceleration or braking. Fortunately, the ESC supports reprogramming via a throttle-based "accept/decline" system typically accessed via a drone remote. In this project, remote input is simulated through software by generating 0% and 100% throttle PWM signals. Following

the steps in appendix 14.3, the ESC is programmed for rapid acceleration and braking behavior [2], which is required for this project.

6.3 Battery

To power the ESC and BLDC, the chosen battery must satisfy both the voltage and current requirements specified in section 6.1. While it is technically possible to use standard AA batteries, this approach introduces significant practical limitations.

A suitable solution is a 3-cell LiPo (Lithium Polymer) battery, which provides a nominal voltage of 11.1 V and 12.6 V when fully charged. However, LiPo batteries pose safety risks, such as fire or explosion, especially in high-impact scenarios like rocket crashes.

The used motor draws 24 A at peak [5], with this information the required discharge rate (C-rating) of the LiPo battery can be calculated. Limiting the battery capacity to a minimum of 1 Ah, the resulting discharge rate would be at least 24 C [6]. Therefore, any 3-cell LiPo battery with a capacity above 1 Ah and a discharge rating of at least 24 C is suitable for powering the BLDC motor. The chosen battery for the project is the 3-cell Vapex 11.1 V 1000 mAh 25 C LiPo battery [8].

While a battery with a larger C-rating or battery capacity could potentially be used, the physical size and weight introduced limitations with the rocket design as described in section 4.

7 Motor torque

The motor reaches near maximum capability with the use of one nut and bolt in each hole of the reaction wheel. From this, the theoretical moment of inertia from the motor and reaction wheel is calculated. The inertia is used in both an unsuccessful and successful attempt, estimating the torque produced by the motor and reaction wheel. By using Newton's third law, the torque is in turn used to estimate the angular acceleration of the rocket caused by the motor and reaction wheel.

7.1 Theoretical moment of inertia

The moment of inertia of a reaction wheel is estimated theoretically by summing the contributions from its components: the plastic base, treated as a solid cylinder, and the mounted bolt-nut pairs approximated as a hollow cylinder.

The plastic base has a mass of 15 g and a radius of 31.75 mm. Its moment of inertia is calculated using the formula for a solid cylinder as shown in eq. (4).

$$I = \frac{1}{2}MR^2 \approx 7.56 \cdot 10^{-6} \text{ kg} \cdot \text{m}^2 \quad (4)$$

The bolt-nut pairs are treated as a hollow cylinder with a mass of 37 g, an inner radius of 25 mm, and an outer radius of 32 mm. The moment of inertia for the bolt-nut pairs is calculated in eq. (5).

$$I = \frac{1}{2}M(R_1^2 + R_2^2) \approx 3.13 \cdot 10^{-5} \text{ kg} \cdot \text{m}^2 \quad (5)$$

In addition to the inertia contributed by the reaction wheel, the BLDC motor also contributes to the total moment of inertia. The motor's outer housing has an inner radius of 11.5 mm and an outer radius of 14.25 mm. In combination with its mass of 37 g, its moment of inertia is calculated using the same formula as in eq. (5), yielding an inertia contribution of $6.20 \cdot 10^{-6} \text{ kg} \cdot \text{m}^2$.

This results in a total theoretical moment of inertia of $4.51 \cdot 10^{-5} \text{ kg} \cdot \text{m}^2$. Despite geometric simplifications, the bolt-nut pairs in the circumference dominate the total moment of inertia contribution, as shown in the calculations.

7.2 Unsuccessful Attempt at Torque Estimation

To estimate the torque produced by the motor and reaction wheel, the motor holder is placed on an inverted pendulum, that includes a high-resolution encoder for determining angular acceleration. From Newton's third law, the torque generated by the BLDC motor and reaction wheel is equal and opposite to the torque observed on the pendulum. This fact is used in eq. (6), where the torque generated by the reaction wheel is applied to the pendulum.

$$\alpha_{wh} \cdot I_{wh} = -\alpha_{pen} \cdot I_{pen} \quad (6)$$

The inertia of the pendulum I_{pen} is determined, using the torque formula in eq. (1), by applying a constant torque, determining the acceleration then calculating the inertia.

For the determination of the reaction wheel's acceleration α_{wh} , a custom-made encoder is created by adding small holes in the reaction wheel, that together with an IR diode and phototransistor will give its relative position with time stamps. In post-processing, the relative position and time stamps could be differentiated twice to find the acceleration of the reaction wheel α_{wh} , which is needed for determining its torque. However, the acceleration became too noisy and unusable in post-processing due to the resolution being too low. Consequently, the experiment is deemed unsuccessful.

7.3 Torque Estimation Using Load Cell

To address earlier estimation challenges, a 5 kg load cell is used to measure the torque. The experimental setup consists of a motor and reaction wheel fastened to the load cell. This configuration effectively formed a cantilever arm structure extending from a stiff base.

The load cell is first calibrated using known weights of incremental mass, yielding a corresponding output voltage. Using this small dataset of mass-voltage pairs, a linear regression model is fitted to establish a relationship between applied load and the equivalent mass.

7.3.1 Step Input Response

Initial tests are conducted by applying a step input to the reaction wheel system: starting at 0% PWM, changed to 50% PWM, and then returned back to 0% PWM after acceleration.

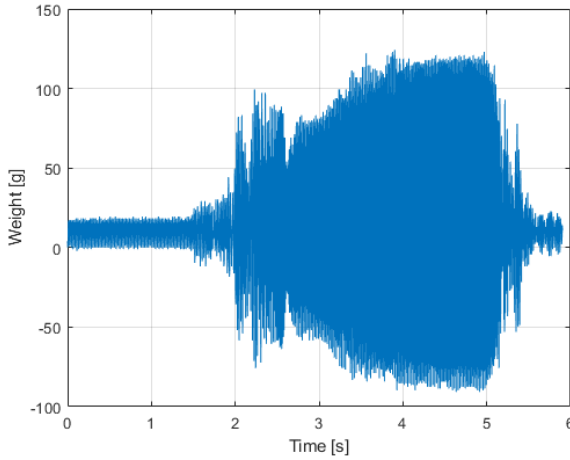


Figure 8: Load cell response during system test with PWM stepping from 0% to 50% and back to 0%.

As shown in fig. 8, the initial results is unsatisfactory due to mechanical vibrations, which generate noise that obscures the signal.

7.3.2 Frequency Analysis and Velocity Profile

To investigate the sources of the noise, further tests are conducted at constant 50% and 100% PWM. A FFT (Fast Fourier Transform) analysis of the data reveals dominant frequency peaks at approximately 184 Hz for 50% PWM and 209 Hz for 100% PWM. Using the assumption that angular velocity is proportional frequency of the noise, the angular velocity can be calculate using the formula $\omega = 2\pi f$. The corresponding angular velocity for the two frequency peaks of 184 Hz and 209 Hz are then respectively 11040.81 RPM and 12540.92 RPM¹. These results highlight two key points: (1) the calculated maximum RPM is slightly below the motors rated maximum 13200 RPM [5], which is expected due to the added inertia of the reaction wheel; and (2) the relationship between PWM input and angular velocity is not proportional, as 50% PWM does not yield 50% of the maximum speed. These tests support the assumption, that the frequency of the noise is proportional with the angular velocity.

Performing a spectrogram on the data from fig. 8 shows the expected velocity curve when applying the 50% PWM step input as seen in fig. 9.

¹Angular velocity (rad/s) can be converted to RPM by multiplying with 9.55.

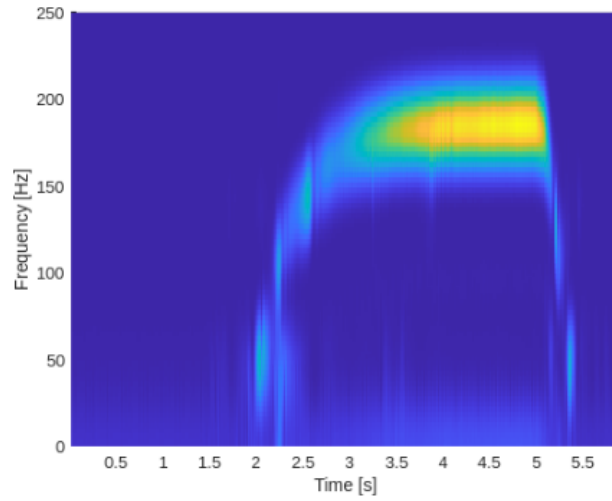


Figure 9: Spectrogram of load cell response when applying a step input of 50% PWM

From fig. 9 the time it takes to reach the step input from 0% is longer than the time decelerating from 50% to 0%. This indicates the deceleration produces a larger torque.

By projecting the peaks of the spectrogram onto the frequency and time plane, an exponential decay function can through trial and error be fitted to the data as shown in fig. 10. From the function the time constant 0.4167 s is found. Furthermore taking the derivative of the function yields the corresponding expected acceleration profile, with a max acceleration of 2763.6 rad/s^2 .

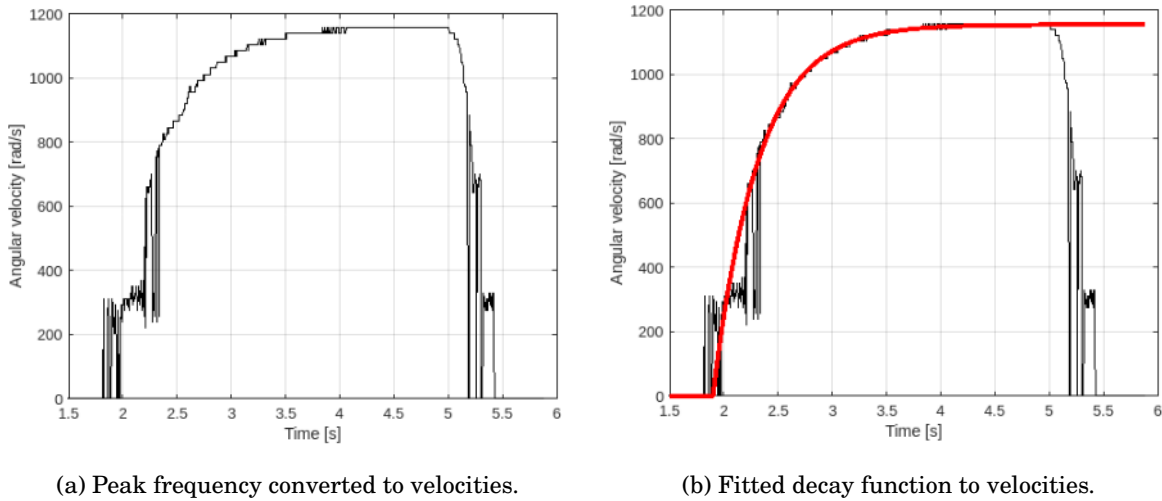


Figure 10: Figure showing velocity curve and fitted velocity curve.

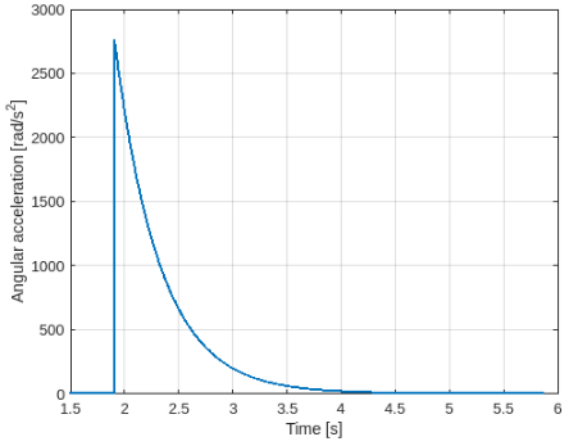


Figure 11: Derived acceleration profile.

The maximum torque generated by a reaction wheel can now be calculated by use of the torque formula in eq. (1) by multiplying the reaction wheel inertia of $4.51 \cdot 10^{-5} \text{ kg} \cdot \text{m}^2$ with the estimated maximum acceleration, from fig. 11, of 2763.6 rad/s^2 . A rough torque estimate of 0.1246 N m is obtained.

7.3.3 Rocket's Angular Acceleration Estimate

Newton's third law can be used to estimate the estimated torque's impact on the rocket's angular acceleration, and thus the capability of a reaction wheel to change the rocket's trajectory. To calculate this angular acceleration of the rocket, an estimate of its moment of inertia must be calculated. For this, the rocket is assumed to be a cylinder with rotational roll and pitch axes at the absolute center of the rocket. At time = 0, the rocket is heaviest, weighing 1.68 kg, measuring 64.5 cm from top to bottom with a radius of 4.75 cm, which can be used in eq. (7) to calculate the rocket's moment of inertia.

$$I = \frac{1}{4} \cdot M \cdot R^2 + \frac{1}{12} \cdot M \cdot L^2 \quad (7)$$

Test four, later shown in section 10.6, is used to evaluate the rocket's angular acceleration, as it only uses one motor and has an unregulated axis from which a constant angular acceleration of 4.28 rad/s^2 is found. This angular acceleration is assumed to be the natural unaffected angular acceleration which, the reaction wheel must counteract. Consequently, the rocket's height and

weight are reduced to 1.275 kg and 53.1 cm, due to the missing motor and battery module. This results in a moment of inertia estimate of 0.03068 kg m^2 using eq. (7).

The torque found in section 7.3.2 is 0.1246 Nm. By solving for acceleration in $\tau = I \cdot \alpha$, the resulting acceleration on the rocket generated by the reaction wheel is 4.06 rad/s².

These two angular accelerations will be discussed further in section 11.6.

8 IMU

In this project, the IMU ST-LSM6DS3, located in the nose cone, is used to determine the rocket's angular position during the acceleration phase. The IMU accelerometer and gyroscope are configured for this use-case with an accelerometer measurement range of $\pm 16\text{ g}$ and a gyroscopic measurement range of 1000 dps . The two data streams are combined using a complementary filter that utilizes a 98% gyroscope- and 2% accelerometer proportion for angular position estimation, improving orientation and reducing drift.

8.1 Accelerometer

Accelerometers are capable of measuring rapid movements but produce noisy data. To reduce this noise, a low-pass filter can be applied, which effectively diminishes high-frequency noise. However, such filtering also suppresses rapid changes in motion, reducing the sensor's responsiveness.

8.1.1 Project Accelerometer Configuration

In this project, the accelerometer on the IMU is configured using the register mappings provided in the datasheet [16, pp. 53–54]. The accelerometer is set to operate with a sample rate of 1.66 kHz, and an anti-aliasing filter can be applied with different cutoff frequencies at a maximum of 400 Hz. The sample rate of 1.66, kHz is chosen through initial testing, that showed sufficient resolution for capturing fast changes with the compatible anti-aliasing filter described in section 8.1.2. A measurement range of $\pm 16\text{ g}$ allows the accelerometer to detect high acceleration values but reduces its sensitivity.

In this project, the measurement range cannot be set lower than $\pm 16\text{ g}$ since testing showed that the acceleration exceeds $\pm 8\text{ g}$ as shown in section 10.2.

The raw output data from the accelerometer cannot be used directly for processing. According to the datasheet, the sensitivity for the range $\pm 16\text{ g}$ is $0.488 \frac{\text{mg}}{\text{LSB}}$ [16, p. 20]. This sensitivity provides the factor needed to convert raw digital output into physical acceleration.

8.1.2 Anti-aliasing filter

An anti-aliasing filter is a low-pass filter connected to the input of the ADC (Analog-Digital Converter). With the anti-aliasing filter applied, noise from high-frequency sources will be re-

duced when reaching above the assigned cutoff frequency which ranges from 50 Hz to 400 Hz [3]. These ranges are explored in testing section 10.7.

8.2 Gyroscope

To stabilize a rocket at a certain angle during the acceleration phase, a gyroscope is essential for providing angular changes and thereby an orientation. This information is required to regulate the rocket to a specific target angle. The gyroscope is subject to drift, which becomes a significant issue when collecting data over longer durations. The rocket acceleration phase is short, thus the drift is minimal and the error has limited time to accumulate. However, the system setup phase is time-consuming which allows the gyroscope to drift. This issue is compensated by use of a complementary filter, as described in section 8.3.

8.2.1 Project gyroscope configuration

In this project, the gyroscope on the IMU is used to determine the current angle of the rocket relative to the target angle of 90° in both the X- and Y-axis. However, due to the orientation of the IMU within the rocket, this is interpreted internally by the IMU as a target angle of 0°.

For this project, the gyroscope is configured to match the accelerometer sampling rate of 1.66 kHz, and to use a measurement range of 1000 dps (Degrees Per Second) with a sensitivity of $35 \frac{\text{mdps}}{\text{LSB}}$, enabling precise conversion of raw output data to angular velocity.

8.3 Complementary filter

The accelerometer and gyroscope each have different errors that must be minimized to obtain reliable data. A complementary filter can help reduce these issues by combining data from both sensors. The filter applies weights to each sensor output, making it possible to control how much each sensor contributes to the final angle estimate.

For this setup the weight of 98% from the gyroscope data and 2% from the accelerometer is used. By combining from the accelerometer with the gyroscope, it becomes possible to provide an external reference for orientation based on the gravitational acceleration. This helps correct any initial angle offset and improves the accuracy of orientation estimation at the moment of launch. To compute this reference, eq. (8) and eq. (9) are used to derive angular orientation estimates for roll and pitch from the accelerometer readings.

$$\text{accelerometer angle}_{roll} = \text{atan2}(a_Y, \sqrt{a_X^2 + a_Z^2}) \cdot \frac{180}{\pi} \quad (8)$$

$$\text{accelerometer angle}_{pitch} = \text{atan2}(-a_X, \sqrt{a_Y^2 + a_Z^2}) \cdot \frac{180}{\pi} \quad (9)$$

Here, a_X , a_Y , and a_Z represent the accelerometer measurements along the X-, Y-, and Z-axis.

The multiplication by $\frac{180}{\pi}$ converts the result from radians to degrees.

9 Controller

The rocket's stabilization relies on a PD controller that controls the reaction wheels based on IMU feedback. This ensures stability by correcting angular deviations during acceleration phase.

9.1 PD Controller

The stabilization system in this project relies on a PD controller regulating the BLDC motors, where the IMU provides continuous angular feedback. A black-box method is used, since no physical model is derived to help with error estimation.

The PD controller regulates the rocket's orientation about the X- and Y-axis by minimizing the angular error from the target angle. For a vertical launch, the target angle is 0° .

Only proportional (P) and derivative (D) terms are used. The integral (I) component is excluded, as the control objective involves small angular deviations where integral wind-up could sabotage regulation. The system must respond quickly to disturbances, making PD control more suitable.

The chosen ESC is unidirectional, meaning the controller needs to operate at the idle speed of 50%, which is reflected in fig. 12, where the idle speed is added to the PD output.

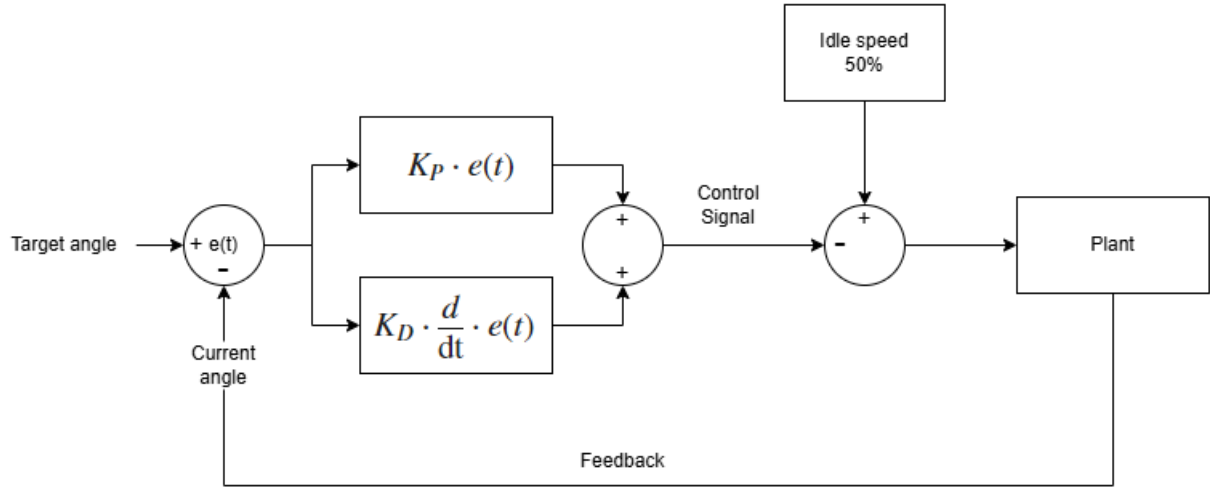


Figure 12: PD Controller Diagram

The proportional gain P determines how powerfully the controller reacts to the angular error. Initial tests indicate that a P value of 12 provides an effective response.

The derivative gain D is tuned to respond to the rate of change of the error, which is essential for counteracting fast disturbances. A value of 3 offers sufficient sensitivity to small angular deviations without overreacting to sensor noise.

10 Testing of Stabilization System

Testing through actual rocket launches has proven to be an essential part of developing the complete rocket stabilization system. These tests have provided valuable insights into the different rocket design choices, onboard electronic choices, and software - including the controller and the IMU data readings. This practical approach has established a foundation for evaluating the current version and identifying areas to improve for the following tests. All graphs are provided in the appendix in an enlarged format for improved readability and detailed analysis.

10.1 Rocket Launch system

The 3D-printed launch system used in testing is primarily based on an available design co-developed by multiple contributors on the online platform Thingiverse [17]. The launch system consists of a base, that is secured to a pallet and the bike pump used to generate air pressure [19]. The nozzle is customized, enabling different nozzle sizes to be 3D printed. The rocket is secured to the launch base using a release mechanism, which is operated via a rope for safe and remote launching [13]. An image of the launch system can be found in appendix 14.1.

10.2 Data Control Test

To determine the appropriate measurement range for the accelerometer, a data control test is conducted. This test served two primary purposes: to identify the optimal measurement range for the accelerometer and to collect baseline data for comparison in future experiments. As expected, the rocket did not follow a vertical trajectory during this test. Nonetheless, the data obtained from the gyroscope proved to be highly reliable, displaying clear and consistent arc patterns across the respective axes, as shown in fig. 13.

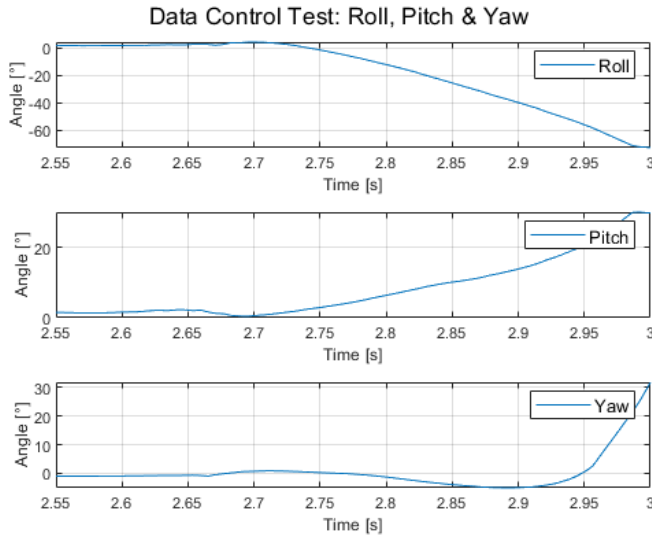
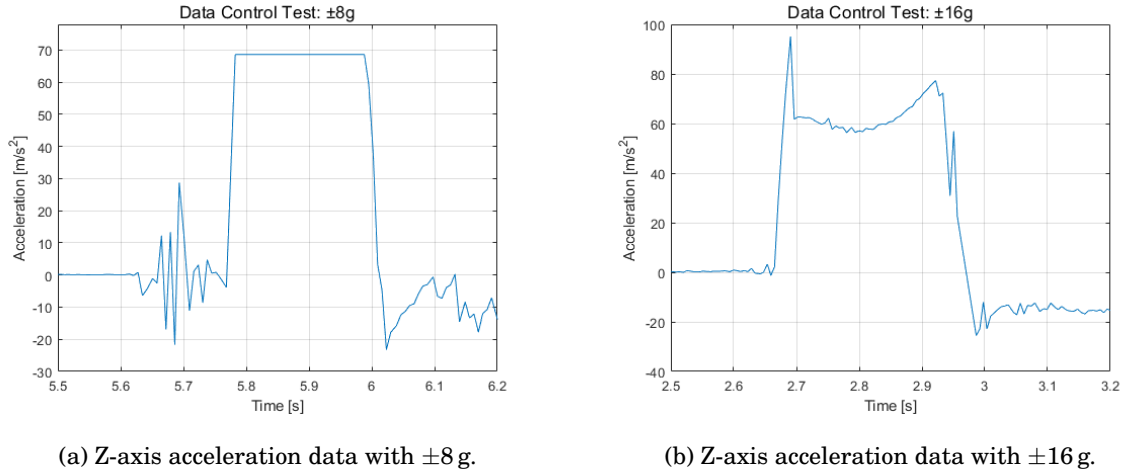


Figure 13: Gyroscope data using a 1000 dps measurement range. Rocket launches at 2.65 s.

The accelerometer is configured with a measurement range of $\pm 8g$. This range provided accurate and usable data for the X- and Y-axis, with recorded values remaining within the limits of the range. However, the acceleration along the Z-axis reached saturation as seen in fig. 14a.



(a) Z-axis acceleration data with $\pm 8g$.

(b) Z-axis acceleration data with $\pm 16g$.

Figure 14: Accelerometer data from the data control test.

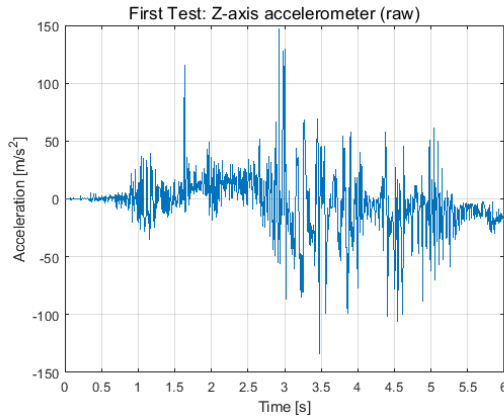
Detailed graphs of fig. 14 with X and Y acceleration can be seen in appendix 14.4. Due to the saturation observed in the Z-axis data, future tests will employ a measurement range of $\pm 16g$ to ensure full capture of high acceleration and avoid data clipping.

10.3 First Test of the Stabilization System

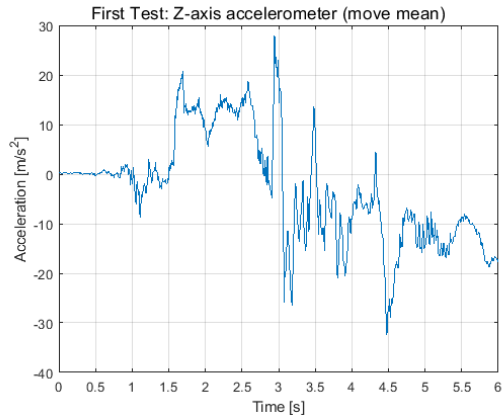
An iterative approach is applied, aiming to gather sufficient data and identify potential errors from each launch. This strategy allows for extensive insight into the launch setup and provides valuable data to support further development of the stabilization system.

The first test confirmed that the modular rocket design with a single battery and motor cylinder, regulating the pitch axis, could be launched successfully without failures during flight. However, it also highlighted the effects of crash landings, as several 3D-printed modules required replacement. Notably, the soldering breadboard used in the test broke, emphasizing the need for the lid in the nose cone.

The Z-axis accelerometer showed an excessive amount of noise which obscured the data to the point where the acceleration start and stop can not unanimously be determined. Filtering the data with a move mean, this can be seen in fig. 15b.



(a) Raw Z-axis acceleration data.



(b) Z-axis acceleration data with move mean.

Figure 15: Accelerometer data from the first test.

From fig. 15b the acceleration phase is determined to be from 1.6 s to 2.6 s.

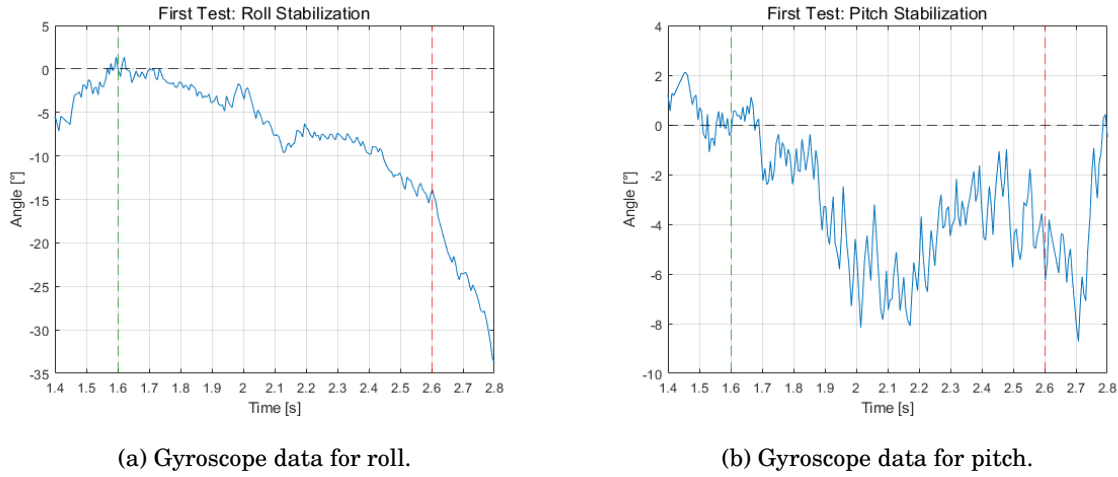


Figure 16: Gyroscope data from the first test.

The roll and pitch angle from 1.6 s to 2.6 s can be seen in fig. 16. These measurements also contain noise, as they are affected by the accelerometer data through the complementary filter. The angle on the unregulated roll axis in fig. 16a keeps increasing, which is expected when no regulation happens. The regulated pitch axis stays within +4° and -8°, which can be seen in the video [11].

Following this test, future development will focus on implementing data logging for the PD controller signals, and the IMU setting is changed to accommodate the noise issue. The additional data logging will enable detailed analysis of the regulation process, indicating the timing and axis of each regulation event.

10.4 Second Test of Stabilization System

In the second test, both motors are implemented to evaluate the stabilization system's ability to regulate motion along both the roll and pitch axis. However, the rocket only ascended approximately 2–3 meters while following an arced trajectory. This limited lift-off highlighted a fundamental design issue: the rocket nozzle is too narrow with its 7 mm diameter, limiting the thrust as seen in video [12]. A wider nozzle is required to allow more efficient acceleration.

10.5 Third Test of Stabilization System

The third test uses both roll and pitch axis regulation. To address the limited thrust observed in the second test, the nozzle diameter is increased to 16 mm. This is shown in fig. 17, which

displays the Z-axis acceleration data, where the time axis span from just before the launch to the end of the acceleration phase.

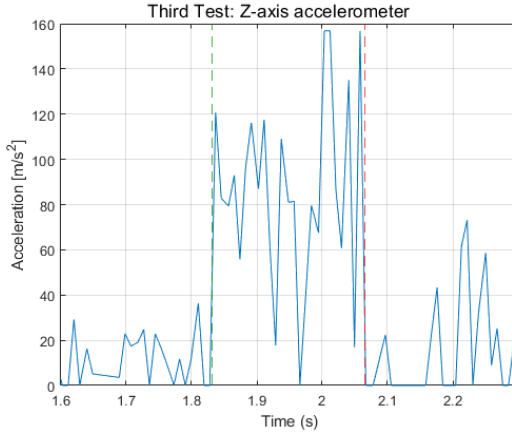
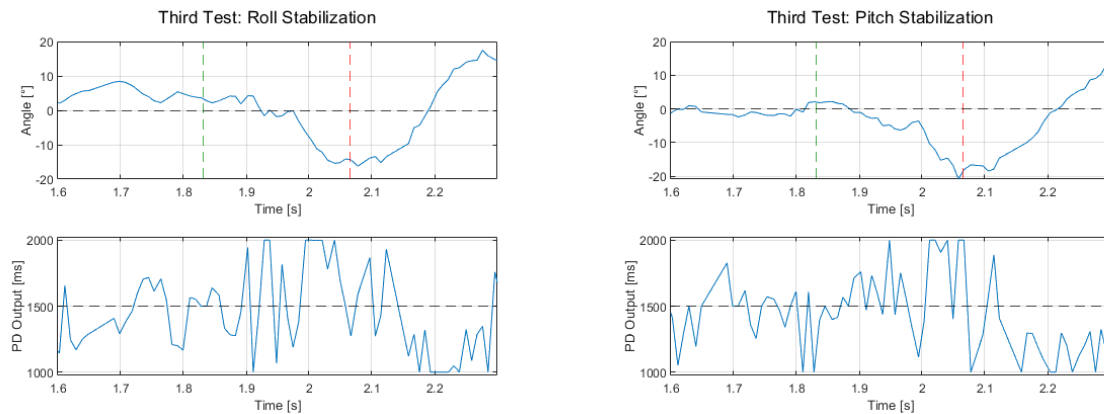


Figure 17: Z-axis acceleration data from the third test launch

Two distinct acceleration peaks can be observed in fig. 17. The first occurs at approximately 1.8 seconds, coinciding with the release of the release mechanism. The second peak is the air phase, at around 2.0 seconds. Here the rocket runs out of water, and the remaining pressurized air is rapidly expelled, generating a short but stronger acceleration pulse. This short acceleration phase of approximately a third of a second emphasizes the oversized nozzle diameter, which needs to be decreased slightly.



(a) Gyroscope data and PD controller output for roll.

(b) Gyroscope data and PD controller output for pitch.

Figure 18: Gyroscope data and PD controller responses from the third test.

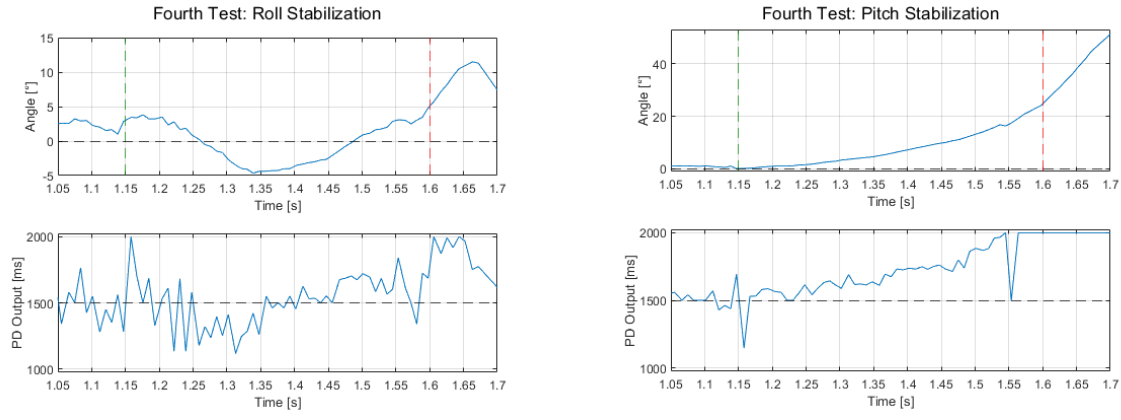
In the first two thirds of the acceleration the rocket roll and pitch angle stays within 10° but then deviate as seen from fig. 18. The PD signal is inverted in software in this test instead of switching two motor wires. This test was the last with two motors, as one broke due to the hard crash landing.

10.6 Fourth Test of Stabilization System

In the fourth test, the nozzle diameter is reduced to 11 mm to counteract the excessive thrust in the third test. The adjustment aimed to extend the duration of the acceleration phase, thereby providing a longer time window for the stabilization system to operate. However, the air pressure used in this test is too high at 8 bars, resulting in deformation of the soda bottle.

Due to a defective ball bearing in the pitch axis motor, only the roll axis module is active during this test. The complementary filter is configured to rely exclusively on the gyroscope data, completely disabling input from the accelerometer. This configuration is chosen to test the stabilization system's behavior, when solely relying on angular velocity being integrated into an angular position, effectively eliminating potential disturbances from the accelerometer caused by the motor.

Despite this limitation, the gyroscope data indicated effective stabilization along the controlled roll axis. As shown in fig. 19a, the rocket's roll angle remained close to zero degrees during flight, and the PD controller output suggests that the reaction wheel actively compensated for deviations in the vertical heading.



(a) Gyroscope data and PD controller output for roll.

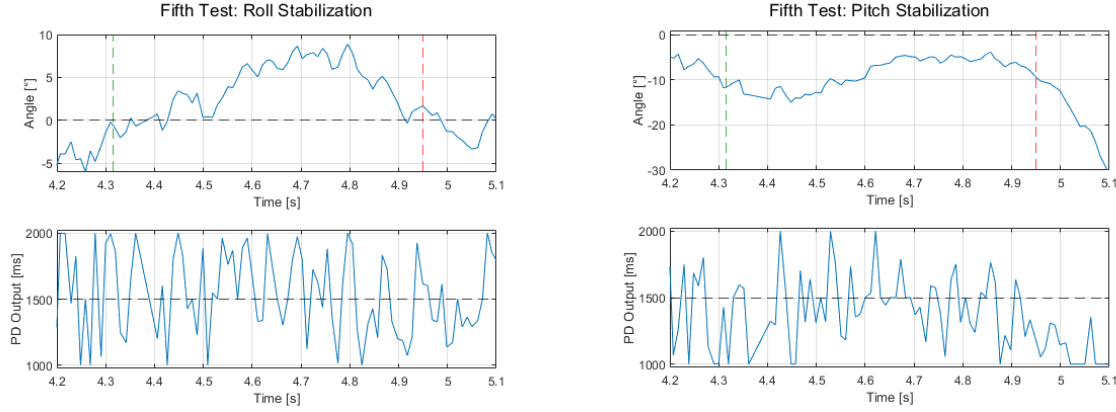
(b) Gyroscope data and PD controller output for pitch.

Figure 19: Gyroscope data and PD controller responses from the fourth test.

In contrast to the possible functional control, the pitch axis remained uncorrected throughout the flight, as expected. The motor module for the pitch axis is removed due to the bearing defect, but nevertheless the PD controller generated appropriate correction signals without a physical effect, as seen in fig. 19b.

10.7 Fifth Test of Stabilization System

For the fifth test, the rocket is only regulated on the roll axis and with a 11 mm nozzle. The test utilized the accelerometer with the complementary filter again. To combat the noise from the motor, the anti-aliasing filter cutoff frequency is set to 50 Hz which previously was 400 Hz.



(a) Gyroscope data and PD controller output for roll.

(b) Gyroscope data and PD controller output for pitch.

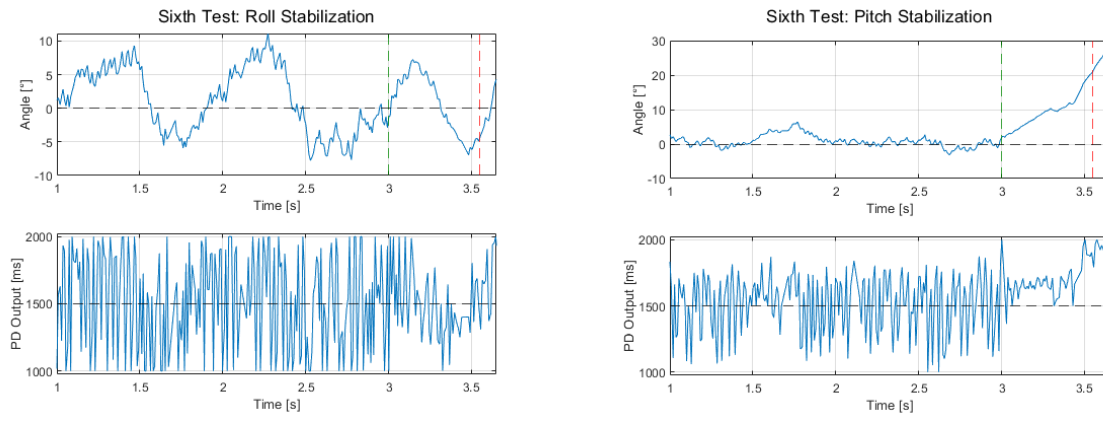
Figure 20: Gyroscope data and PD controller responses from the fifth test.

During the acceleration phase, in the span of half a second, the roll angle varies between -4° and $+8^\circ$ as seen in fig. 20a.

The unregulated pitch angle, starts at -5° and stays in that heading for the remaining acceleration time, and is not corrected as expected.

10.8 Sixth Test of Stabilization System

With the fifth test showing promising results the sixth test utilized the same settings and setup. The launch starts at 3 seconds, where the increasing roll angle is adjusted, as seen between the marks indicating the acceleration phase on fig. 21a. These adjustments correlate with the PD output seemingly moving in the positive pulse widths along with the angle, as seen in the PD output for roll in fig. 21a. This correlation indicates, that the reaction wheel might help regulate the heading towards a 0° angle as desired.



(a) Gyroscope data and PD controller output for roll.

(b) Gyroscope data and PD controller output for pitch.

Figure 21: Gyroscope data and PD controller responses from the sixth test.

Prior to the launch, a wobble stemming from the rocket launch platform can be seen in fig. 21a. This wobble is reflected on the PD output for roll in fig. 21a, that changes between the maximum- and minimum pulse width rapidly.

In fig. 21b the pitch angle increased during the entire acceleration phase, as there is still no motor on this axis. When the rocket crash landed it broke the last motor, thus concluding the testing.

11 Discussion

In this project, it is not definitively known whether a successful launch is entirely dependent on the regulator's performance, even though the data suggests the rocket's regulation is functioning correctly. However, it is evident that the regulator influences the rocket's behavior as seen when the motors are absent, there is a noticeable deviation in the trajectory, indicating that reaction wheel based regulation plays a significant role. Furthermore, the primary limitations are time constraints and hardware durability. Frequent structural failures required repeated 3D printing, which significantly slowed progress. Additionally, motor and ESC failures required repair or replacement between tests, further hindering the project.

11.1 RTOS

To enhance the responsiveness and efficiency of the control system, future implementations of the project should be using the real time operating system FreeRTOS. This would allow the system to manage simultaneous tasks with different priorities, improving performance and timing accuracy. For example, the following tasks could be defined:

- High Priority: IMU task (sensor data acquisition)
- Medium Priority: PD regulator task (motor control)
- Low Priority: SD card task (data logging)

This multitasking approach would provide real-time responsiveness, replacing the current sequential execution method and improving execution time.

11.2 Launchpad changes

Though the rocket launch system [13] has been a great help in the initial tests, it needs some improvement. The wobble seen in section 10.8, is caused by the insufficient stability of the 3D-printed base. To give the rocket the best start conditions this needs to be addressed. A simple solution for the existing launch system could be to implement three posts to prevent wobble.

11.3 Force and Pressure Measurement

During the testing of the stabilization system, no standardized measurements for the amount of water or applied pressure are documented. Incorporating consistent water and pressure measurements from the beginning could have improved the quality and comparability of the test data. Future tests should include measurements of these parameters to reduce uncertainty and enhance the comparability of data across multiple launches.

11.4 Fully Integrated Water Rocket Design

Consistent crashing throughout testing caused the 3D-printed components and motor to break. Furthermore, the limited pressure tolerance of standard 2 L soda bottles, caused the bottles to deform. To address these challenges, alternative materials should be considered.

Future rocket design should utilize materials with increased impact resistance, to maintain the rocket's structural and hardware integrity when crashing. Additionally, an internal parachute deployment system could be implemented to ensure a safe descent, thereby minimizing impact forces and increasing the likelihood of electronic component survival after landing.

The pressure of 8 bars, as seen in test 4 section 10.6, highlighted the need for a custom lightweight water chamber to withstand higher pressures, eliminating the separation issues of the mold and bottle when reaching high pressure.

11.5 BLDC motor and ESC

The fixed idle speed of 50% is not optimal, as it can be seen from section 7.3.2, where the non-proportional relationship between PWM and RPM is highlighted. Additionally, the acceleration- and breaking duration is significantly different as seen in fig. 10, which causes different torque applications. This would be solved by using a bidirectional ESC, which would allow an idle speed of 0% PWM and an identical acceleration profile in both directions and minimize motor saturation. Furthermore, noise generated from the unidirectional 50% idle speed will be eliminated if the bidirectional ESC is used.

Combining a bidirectional ESC implementation with a new BLDC motor with larger torque would increase the load- and acceleration possibilities. This would allow a larger reaction wheel inertia to be driven by the ESC and BLDC motor, thereby influencing a larger generated torque

on the rocket.

11.6 Torque Estimation

Determination of the generated torque by the reaction wheel faced multiple challenges in this project, where the only estimation utilized a function fitted to a spectrogram. The reaction wheel acceleration estimated, in conjunction with the theoretical moment of inertia, gave a rough estimate of the torque. These approximations are subject to uncertainty, therefore a better estimation should be found. Preferably the noise, that obscured the data collected from the load cell, should be removed making the intended use of the load cell possible. This could be by manufacturing a completely new reaction wheel with better symmetry, practically eliminating oscillation. The force applied to the load cell would then form the basis for calculating the applied torque, providing valuable insight into the capabilities of the reaction wheel. In addition, this would help clarify the effectiveness of the reaction wheels during launches.

The torque is not the only estimation which should be revisited, as the rocket's theoretical inertia of 0.03068 kg m^2 is based on assumptions. Additionally, the natural unaffected acceleration, found to be 4.28 rad/s^2 , is only based on a single test and should be thoroughly tested for validation.

With these estimation uncertainties in mind, the resulting acceleration on the rocket made by the reaction wheel is 4.06 rad/s^2 , while the natural acceleration is 4.28 rad/s^2 . These values are roughly the same size at the start of a launch ($t = 0$). By the end of the acceleration phase, the rocket has lost its water weight, which shifts the relation in favor of the reaction wheel.

11.7 Complementary Filter

The use of a complementary filter presents both advantages and disadvantages. In the fourth test section 10.6, the complementary filter is removed, resulting in no noise from the accelerometer being passed to the gyroscopic angle measurement. This resulted in a clearer and more accurate angle measurement, improving the stability of the regulation response.

However, the vertical reference provided by the accelerometer is crucial during the rocket's acceleration phase, as it helps maintain a vertical trajectory. Therefore, an optimal solution may involve implementing logic to deactivate the complementary filter when a certain threshold of Z-axis acceleration is reached, thus allowing usage of the vertical reference and gathering reli-

able gyroscope readings.

11.8 IMU Evaluation

A higher sampling rate is preferable to capture the motion of the rocket during this brief acceleration phase. The current IMU, the ST-LSM6DS3, supports output data rates of 3.33 kHz and 6.66 kHz.

However, at these data rates, the internal anti-aliasing filter is automatically bypassed, even though it remains configurable in the register settings. According to the datasheet [16, p. 54], this is due to limitations in the circuit before the ADC, which does not operate effectively at such high bandwidths. As a result, the signal is passed directly to the ADC without analog filtering, which defeats the purpose of the filter even though it is applied. Ultimately, a new IMU should be considered in the future to support higher sampling rates while retaining the use of an internal analog filter if possible, as provided at lower frequencies by the LSM6DS3.

11.9 Controller Evaluation

Testing indicated the regulator, with its current configuration, is capable of reacting to orientation changes, then attempting to redirect the rocket toward a vertical trajectory. Either the reaction wheels' inertia or the acceleration of the motor could be increased, which would generate a large torque, and thus impacting the rocket's trajectory more aggressively.

To put the indications beyond doubt, further repeatable testing is necessary to eliminate the uncertainty between successful corrections by the reaction wheels and a fortunate flight path independent of the regulator. At this stage, all the regulation success have been labeled as indications showing great conceptual potential using reaction wheels for controlling a rocket trajectory.

11.10 Evaluation of the testing

The second test showed limitations of launching the rocket with both motor modules as the rocket had trouble reaching height. This showcased initial trouble with weight, which is further emphasized in the third test, where adjusting the rocket to 0° is challenging. The roll and pitch angle from the third test indicates that the rocket overshot its target angle, assuming that the angle change is caused by the reaction wheels. This could potentially be caused by a nose heavy rocket, where the center of gravity is moved towards the nose cone, resulting in difficulty

when stabilizing the trajectory. However, the angle corrections showed early indications of the reaction wheels actually affecting the rocket's trajectory. The first three tests concluded the regulating for both roll and pitch, as crash landing proved destructive to the motors.

In the fourth test, a single motor is used for launching the rocket, which highlighted the difference between using a reaction wheel and not using one. The regulated roll axis is assumed to show the reaction wheels regulating the trajectory, keeping the trajectory close to vertical as intended. The unregulated pitch axis graph shows an unaffected trajectory without a reaction wheel, which with its parabola like trajectory indicates a constant acceleration in one direction, that is used for comparison with the estimated applied torque described previously.

The fifth test, is also executed with a single motor and reaction wheel, resulted in similar outcome, as the regulated roll axis is also corrected to zero degrees. The unregulated pitch axis is not corrected back to zero degrees as expected, which further highlighted the difference possible impact of regulating with a reaction wheel.

Even though the pitch axis never corrected back to 0 degrees, it remained within 10 °for the duration of the acceleration. This could be caused by the gyroscopic effect, but it is important to note that this remains a hypothesis, as no direct measurements or testing of the gyroscopic effect are done during this project.

Finally, the sixth test showed the exactly same behavior during its acceleration phase, which further supports the indications of a working regulation using reaction wheels.

The regulated roll axis in both the fourth-, fifth- and sixth tests overshot the zero-degree angle when being corrected, which showcases a vulnerability in the current regulating system. The three last tests shows the importance of regulation on both axes. Finally, the estimated applied torque from section 11.7 supports the plausibility of the indicated regulation functioning as intended.

12 Conclusion

It is inconclusive that the stabilization system regulates the rocket into a vertical trajectory since repeated tests of unregulated and regulated launches with higher quality are required. However, this project explored and solved issues with different outcomes, setting the foundation for completing the stabilization system.

The modular design of the rocket proved to be useful when assembling and disassembling before and after launch. It effectively reduced the rebuild time as only the damaged parts needed to be reprinted and replaced rather than the entire rocket structure. To keep the rocket intact, a recovery mechanism, like a parachute, would be favorable for repeatable testing, allowing for better development and optimization of the complete system.

The mold proved to be a good medium between the bottle and the rocket body, but the use of the mold is limited to launches below 8 bars, since the bottle deforms.

The inertia of the reaction wheel fits the motor used in this project, however, the reaction wheel could be tested or optimized further. The only successful torque estimation is obtained from fitting a curve to the noise generated by the reaction wheel oscillating. Improvements are necessary to get a better estimation of the reaction wheel torque.

Improving the reaction wheel's torque measurement will enhance the accuracy of the angular acceleration estimation; however, the rocket's calculated moment of inertia also requires improvement. Additionally, the natural angular acceleration used in the analysis contains uncertainties that must be addressed.

In conclusion, the torque generated from braking and acceleration at 50% idle speed is not equal. If bidirectional ESCs are not available, further testing should be considered to find the torque equilibrium.

The complete system using a single motor module showed indications of effective adjustments to the rocket's trajectory during testing without fins. Nonetheless, further investigation is needed for tests using two active axes on the rocket since indications of a successful regulation is limited. In conclusion, the PD controller is a sufficient choice for regulation. With additional time and improved repeatability in testing, fine-tuning of controller parameters should be considered. Furthermore, the complementary filter enhanced the accuracy of the stabilization system by providing an orientation reference and reducing gyroscopic drift.

Though the stabilization system generally is inconclusive, the regulated axis showed promising results in contrast to the non-regulated axis, where the error was not corrected. However, the complete system testing did not reach the same positive indications due to defects in a motor preventing use of both motors. Consequently, the testing of the rocket's performance mainly showed promising indications of controlling a single-axis trajectory.

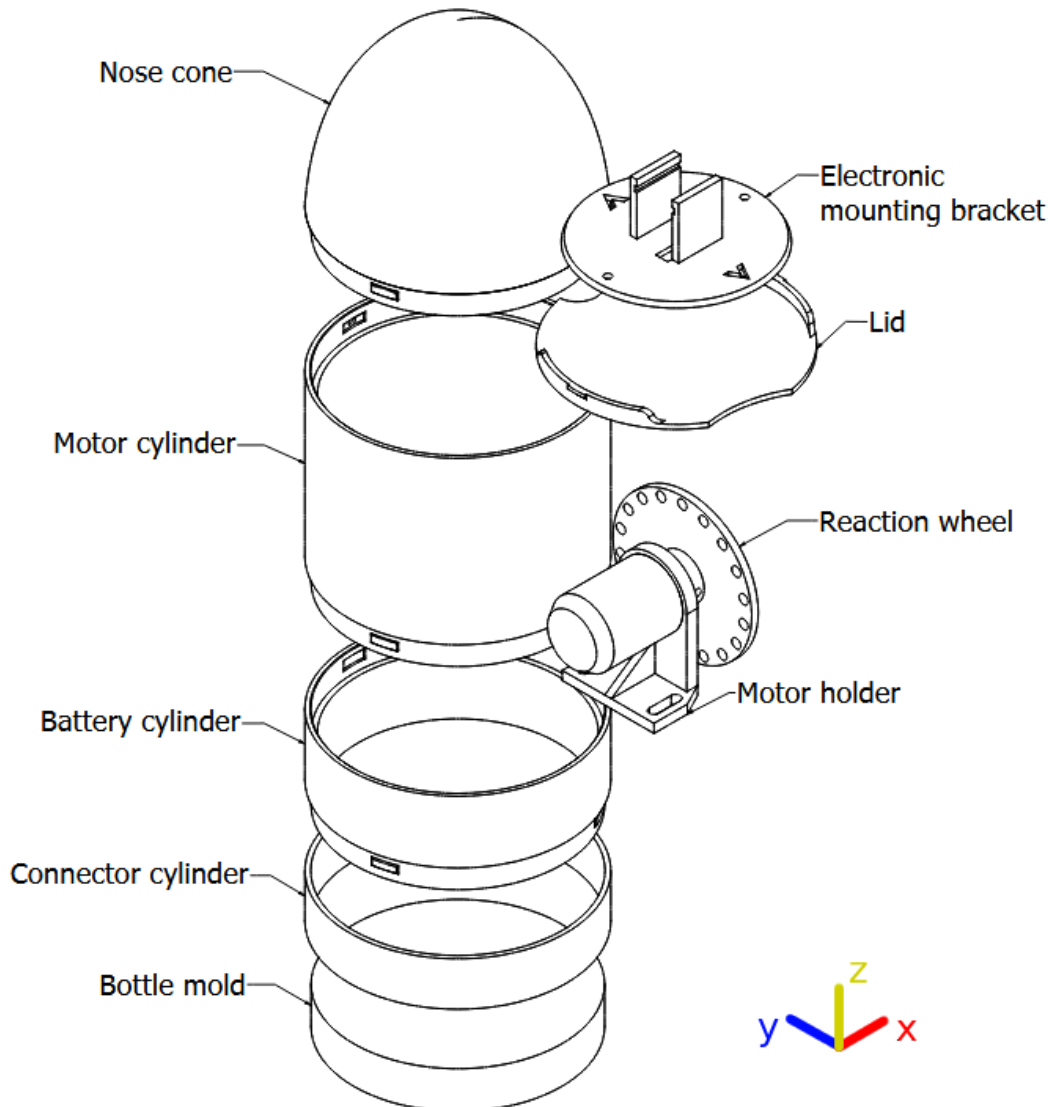
13 Bibliography

- [1] Autodesk. Autodesk Inventor Software. <https://www.autodesk.com/dk/products/inventor/overview>. [Accessed 21-05-2025].
- [2] Conrad Electronic. Datasheet for Reely Sky-Series 20A ESC. <https://asset.conrad.com/media10/add/160267/c1/-/gl/001460685ML00/user-safety-instructions-1460685-reely-sky-series-20a-model-aircraft-brushless-motor-0.pdf>. [Accessed 27-03-2025].
- [3] Digi-Key Electronics. The Basics of Anti-Aliasing Low-Pass Filters. <https://www.digikey.com/en/articles/the-basics-of-anti-aliasing-low-pass-filters>, 2025. [Accessed 18-03-2025].
- [4] Elehobica. FatFs library for Raspberry Pi Pico. https://github.com/elehobica/pico_fatfs, 2025. [Accessed 24-04-2025].
- [5] EMAX. EMAX GT2218/09 1100kv Outrunner Brushless Motor for RC Models. <https://www.banggood.com/EMAX-GT2218-or-09-1100KV-Outrunner-Brushless-Motor-For-RC-Models-p-989039.html>, 2023. [Accessed 25-02-2025].
- [6] Grepow Battery. What is the C Rating on a LiPo Battery? <https://www.grepow.com/blog/what-is-the-c-rating-on-a-lipo-battery.html>, 2023. [Accessed 04-04-2025].
- [7] KIRI Engine. KIRI Engine WEB — kiriengine.app. <https://www.kiriengine.app/web-version/mymodel>. [Accessed 20-05-2025].
- [8] RC Kongen. Vapex 11.1V 1000mAh 25C LiPo Batteri. <https://rckongen.dk/products/vapex-vplp010fd>. [Accessed 20-05-2025].
- [9] Oscar Liang. PWM, PPM and Their Differences. <https://oscarliang.com/pwm-ppm-difference-conversion/>, 2017. [Accessed 15-05-2025].
- [10] Raspberry Pi Ltd. Raspberry Pi pico W datasheet. <https://datasheets.raspberrypi.com/picow/pico-w-datasheet.pdf>. [Accessed 22-05-2025].

- [11] Sebastian Piessenberger. Sdu robotics - water rocket test 1 pitch axis. https://www.youtube.com/watch?v=11JPB92M4Zs&list=PL0yESx9PWsiB_6e26h_a_aPU2y4m0XSPj&index=5. [Accessed 31-05-2025].
- [12] Sebastian Piessenberger. Sdu robotics - water rocket test 2 regulating axis. https://www.youtube.com/watch?v=HudnaXCujlY&list=PL0yESx9PWsiB_6e26h_a_aPU2y4m0XSPj&index=7. [Accessed 31-05-2025].
- [13] poelstra. WRLS (Water Rocket Launch System) by poelstra — thingiverse.com. <https://www.thingiverse.com/thing:4951002/remixes>, 2021. [Accessed 23-02-2025].
- [14] Pololu. Breakout Board for microSD Card. <https://www.pololu.com/product/2597>. [Accessed 29-03-2025].
- [15] RotorDrone Pro. Understanding Kv Ratings. <https://www.rotordronepro.com/understanding-kv-ratings/>, 2023. [Accessed 08-03-2025].
- [16] STMicroelectronics. *LSM6DS3: iNEMO inertial module: always-on 3D accelerometer and 3D gyroscope*, 2017. [Accessed 10-02-2025].
- [17] Thingiverse.com. Thingiverse - Digital Designs for Physical Objects. <https://www.thingiverse.com/>. [Accessed 27-05-2025].
- [18] Ufine Battery. Mastering 3S LiPo Voltage: Your Ultimate Charging Guide. <https://www.ufinebattery.com/blog/mastering-3s-lipo-voltage-your-ultimate-charging-guide/>, 2023. [Accessed 02-04-2025].
- [19] vcom. Launch base large by vcom — thingiverse.com. <https://www.thingiverse.com/thing:5429951>, 2022. [Accessed 25-02-2025].

14 Appendix

14.1 Rocket Design and Launch System





14.2 Videos

14.2.1 Test 1

Test 1 roll axis: https://www.youtube.com/watch?v=bJjiR-lU2Iw&list=PL0yESx9Pwsib_6e26h_a_aPU2y4m0XSPj&index=7

Test 1 pitch axis: https://www.youtube.com/watch?v=1JPB92M4Zs&list=PL0yESx9Pwsib_6e26h_a_aPU2y4m0XSPj&index=6

or in: /Rocket Stabilization System/Videoer/test1

14.2.2 Test 2

video: https://www.youtube.com/watch?v=HudnaXCujlY&list=PL0yESx9Pwsib_6e26h_a_aPU2y4m0XSPj&index=7

or in: /Rocket Stabilization System/Videoer/test2

14.2.3 Test 3

Quick acceleration phase: https://www.youtube.com/watch?v=vyxYovGduDk&list=PL0yESx9Pwsib_6e26h_a_aPU2y4m0XSPj&index=8

The same in slow motion: https://www.youtube.com/watch?v=Tmf3ehmc0yg&list=PL0yESx9Pwsib_6e26h_a_aPU2y4m0XSPj&index=10

or in: /Rocket Stabilization System/Videoer/test3

14.2.4 Test 4

Test 4 roll axis: https://www.youtube.com/watch?v=1JjGm0JXhXM&list=PL0yESx9Pwsib_6e26h_a_aPU2y4m0XSPj&index=5

Test 4 pitch axis: https://www.youtube.com/watch?v=QB_dXZ0NKn4&list=PL0yESx9Pwsib_6e26h_a_aPU2y4m0XSPj&index=4

or in: /Rocket Stabilization System/Videoer/test4

14.2.5 Test 5

Test 5 roll axis: https://www.youtube.com/watch?v=ffjskw5SaDA&list=PL0yESx9Pwsib_6e26h_a_aPU2y4m0XSPj&index=12

Test 5 pitch axis: https://www.youtube.com/watch?v=Z_pKZFIzIhE&list=PL0yESx9Pwsib_6e26h_a_aPU2y4m0XSPj&index=11

or in: /Rocket Stabilization System/Videoer/test5

14.2.6 Test 6

Test 6 roll axis: https://www.youtube.com/watch?v=4gCkk7KvdEE&list=PL0yESx9Pwsib_6e26h_a_aPU2y4m0XSPj&index=2

Test 6 pitch axis https://www.youtube.com/watch?v=1q4m63qPTUI&list=PL0yESx9Pwsib_6e26h_a_aPU2y4m0XSPj&index=11

or in: /Rocket Stabilization System/Videoer/test6

14.3 ESC Programming

User Manual of Brushless Speed Controller

HW-SM003DUL-20150512

Thanks for purchasing our Electronic Speed Controller (ESC). High power system for RC model is very dangerous, please read this manual carefully. In that we have no control over the correct use, installation, application, or maintenance of our products, no liability shall be assumed nor accepted for any damages, losses or costs resulting from the use of the product. Any claims arising from the operating, failure or malfunctioning etc. will be denied. We assume no liability for personal injury, property damage or consequential damages resulting from our product or our workmanship. As far as is legally permitted, the obligation to compensation is limited to the invoice amount of the affected product.

Specifications

Model	Cont. Current	Burst Current (10s)	BEC Mode	BEC Output	BEC Output Capability			Battery Cell	Weight	Size L*W*H
					2S Lipo	3S Lipo	4S Lipo			
Sky-series-6A	6A	8A	Linear	5V/0.8A	3 servos	2 servos		2S 54 cells	5.5g	37*17*4.5
Sky-series-12A	12A	15A	Linear	5V/1A	3 servos	4 servos		2S 54 cells	9g	38*18*6
Sky-series-12E	12A	15A	Linear	5V/2A	5 servos	4 servos		2S 54 cells	10g	38*18*7
Sky-series-15A	15A	20A	Linear	5V/2A	5 servos	4 servos		2S 54 cells	16.5g	48*22.5*6
Sky-series-20A	20A	25A	Linear	5V/2A	5 servos	4 servos		2S 54 cells	19g	42*25*8
Sky-series-30A	30A	40A	Linear	5V/2A	5 servos	4 servos		2S 54 cells	37g	69*25*8
Sky-series-40A	40A	55A	Linear	5V/3A	5 servos	4 servos		2S 54 cells	39g	69*25*8
Sky-series-50A-UJBE	40A	55A	Switch	5V/3A	5 servos	5 servos	5 servos	2S 54 cells	43g	65*25*12
Sky-series-50A-UJBE	50A	65A	Switch	5V/5A	8 servos	6 servos	6 servos	2S 45 cells	41g	65*25*10
Sky-series-60A-UJBE	60A	80A	Switch	5V/5A	8 servos	6 servos	6 servos	2S 45 cells	63g	77*35*14
Sky-series-60A-OPTO	60A	80A	N/A	N/A				2S 45 cells	60g	86*38*12
Sky-series-80A-UJBE	80A	100A	Switch	5V/5A	8 servos	8 servos	6 servos	2S 45 cells	82g	86*38*12
Sky-series-80A-OPTO	80A	100A	N/A	N/A				2S 45 cells	78g	86*38*12

Programmable Items (The option written in bold font is the default setting)

- Brake Setting: Enabled / **Disabled**
- Battery Type: Lipo / NiMH
- Low Voltage Protection Mode(Cut-Off Mode): **Soft Cut-Off (Gradually reduce the output power)** / Cut-Off (Immediately stop the output power)
- High Voltage Protection Threshold(Cut-Off Threshold): Low / Medium / High
1) For lithium battery, the battery cell number is calculated automatically. Low / medium / high cutoff voltage for each cell is: 2.85V/3.15V/(3/2.9V). For example: For a 3S Lipo, when "Medium" cutoff threshold is set, the cut-off voltage will be: 3.15*3=9.45V
- For NiMH battery, low / medium / high cutoff voltages are 0%/50%/65% of the startup voltage (i.e. the initial voltage of battery pack), and 0% means the low voltage cut-off function is disabled. For example: For a 6 cells NiMH battery, fully charged voltage is 1.44*6=8.64V, when "Medium" cut-off threshold is set, the cut-off voltage will be: 8.64*50%=4.32V.
- Startup Mode: **Normal** / Soft / Super-Soft (300ms / 1.5s / 3s)
a) Normal mode is suitable for fixed-wing aircraft. Soft or Super-soft modes are suitable for helicopters. The initial acceleration of the Soft and Super-Soft modes are slower, it takes 1.5 second for Soft startup or 3 seconds for Super-Soft startup from initial throttle advance to full throttle. If the throttle is completely closed (throttle stick moved to bottom position) and opened again (throttle stick moved to top position) within 3 seconds after the first startup, the re-startup will be temporarily changed to normal mode to get rid of the chance of a crash caused by slow throttle response. This special design is suitable for aerobatic flight when quick throttle response is needed,
- Timing: **Low** / Medium / High, (3.75/15/26.25)
Usually, low timing is suitable for most motors. To get higher speed, High timing value can be chosen.

Begin To Use Your New ESC

IMPORTANT! Because different transmitter has different throttle range, please calibrate throttle range before flying.

Throttle range setting (Throttle range should be reset whenever a new transmitter is being used)

Switch on the transmitter, move throttle stick to the top position	Connect battery pack to the ESC, and wait for about 2 seconds	The "Beep-Beep" tone should be emitted, means the top point of throttle range has been confirmed	Move throttle stick to the bottom position, several "beep" tones should be emitted to present the amount of battery cells	Along "Beep" tone should be emitted, means the lowest point of throttle range has been correctly confirmed
Move throttle stick to bottom position and then switch on transmitter.	Connect battery pack to ESC, special tone like 'J 123' means power supply is OK	Several "beep" tones should be emitted to present the amount of lithium battery cells	When self-test is finished, a long "beep" tone should be emitted	Move throttle stick upwards to go flying

Normal startup procedure

- Start up failure protection: If the motor fails to start within 2 seconds of throttle application, the ESC will cut-off the output power. In this case, the throttle stick **MUST** be moved to the bottom again to restart the motor. (Such a situation happens in the following cases: The connection between ESC and motor is not reliable, the propeller or the motor is blocked, the gearbox is damaged, etc.)
- Over-heat protection: When the temperature of the ESC is over about 110 Celsius degrees, the ESC will reduce the output power.

Program the ESC with your transmitter (4 Steps)

Note: Please make sure the throttle curve is set to 0 when the throttle stick is at bottom position and 100% for the top position,

1. Enter program mode
2. Select programmable items
3. Set item's value (Programmable value)
4. Exit program mode

1. Enter program mode

- 1) Switch on transmitter, move throttle stick to top position, connect the battery pack to ESC
- 2) Wait for 2 seconds, the motor should emit special tone like "beep-beep"
- 3) Wait for another 5 seconds, special tone like "♪ 56712" should be emitted, which means program mode is entered

2. Select programmable items

After entering program mode, you will hear 8 tones in a loop with the following sequence. If you move the throttle stick to bottom within 3 seconds after one kind of tones, this item will be selected.

- | | | |
|--------------------------|--------------------|------------------|
| 1. "beep" | brake | (1 short tone) |
| 2. "beep-beep" | battery type | (2 short tone) |
| 3. "beep-beep-beep" | cutoff mode | (3 short tone) |
| 4. "beep-beep-beep-beep" | cutoff threshold | (4 short tone) |
| 5. "beep—" | startup mode | (1 long tone) |
| 6. "beep—beep—" | timing | (1 long 1 short) |
| 7. "beep—beep-beep—" | set all to default | (1 long 2 short) |
| 8. "beep—beep—" | exit | (2 long tone) |

Note: 1 long "beep——" = 5 short "beep"

3. Set item value (Programmable value)

You will hear several tones in loop. Set the value matching to a tone by moving throttle stick to top when you hear the tone, then a special tone "♪ 1515" emits, means the value is set and saved. (Keeping the throttle stick at top, you will go back to Step 2 and you can select other items; or moving the stick to bottom within 2 seconds will exit program mode directly)

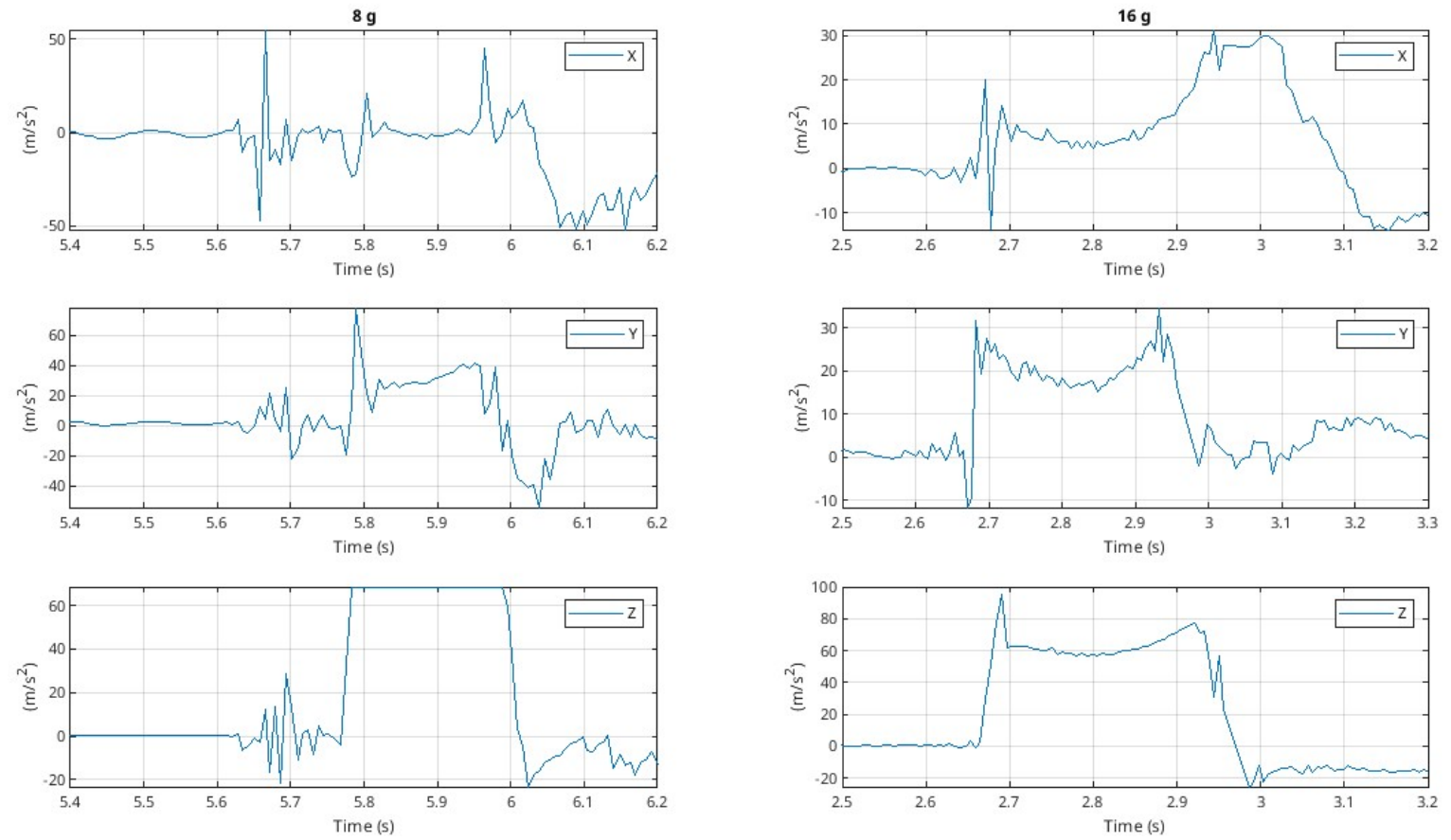
Items	Tones "beep—" 1 short tone	"beep-beep—" 2 short tones	"beep-beep-beep—" 3 short tones
Brake	Off	On	
Battery type	Lipo	NiMH	
Cutoff mode	Soft-Cut	Cut-Off	
Cutoff threshold	Low	Medium	High
Start mode	Normal	Soft	Super soft
Timing	Low	Medium	High

4. Exit program mode

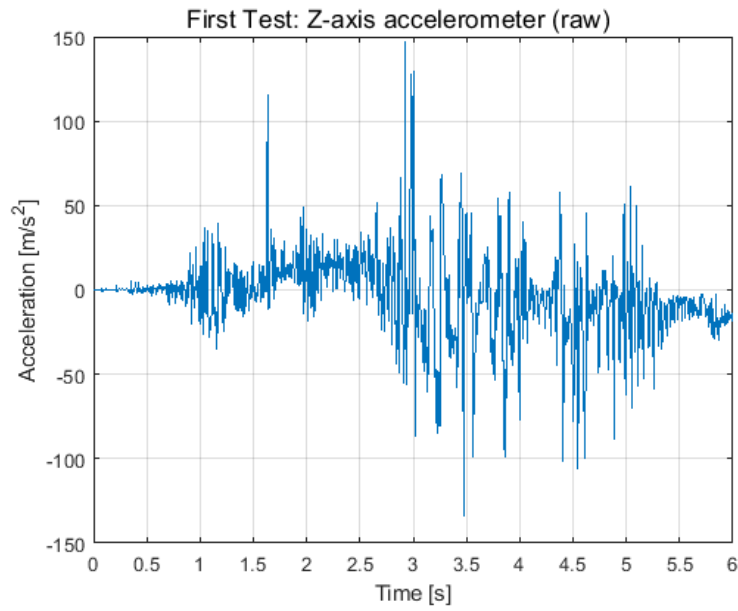
There are 2 ways to exit program mode:

1. In step 3, after special tone "♪ 1515", please move throttle stick to the bottom position within 2 seconds.
2. In step 2, after tone "beep—beep—"(th at is: The item #8), move throttle stick to bottom within 3 seconds.

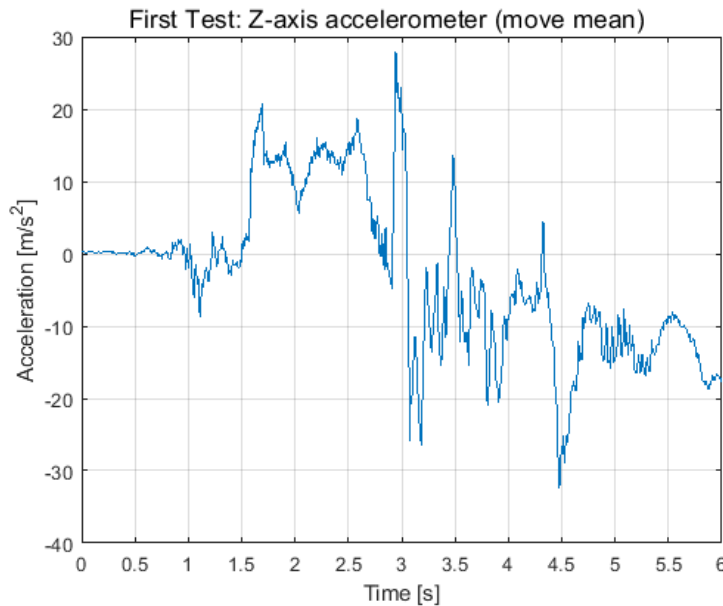
14.4 Data Control Test Graphs



14.5 First Test Graphs

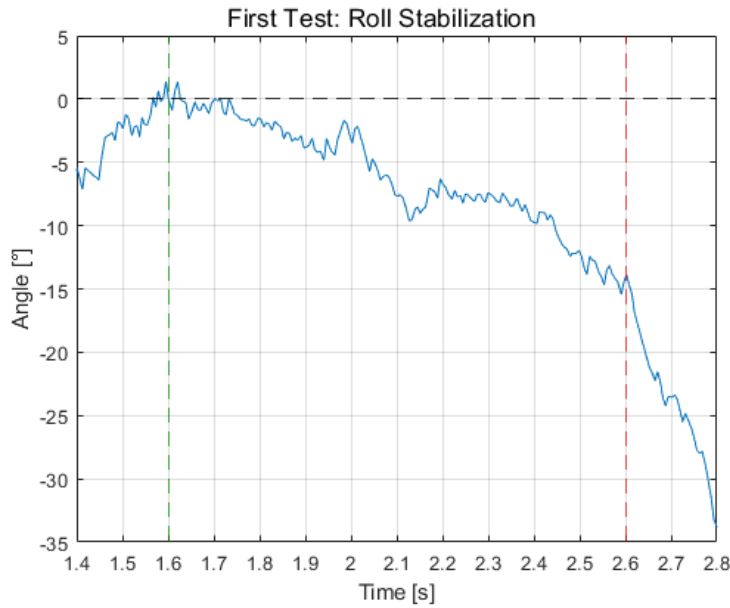


(a) Raw Z-axis acceleration data.

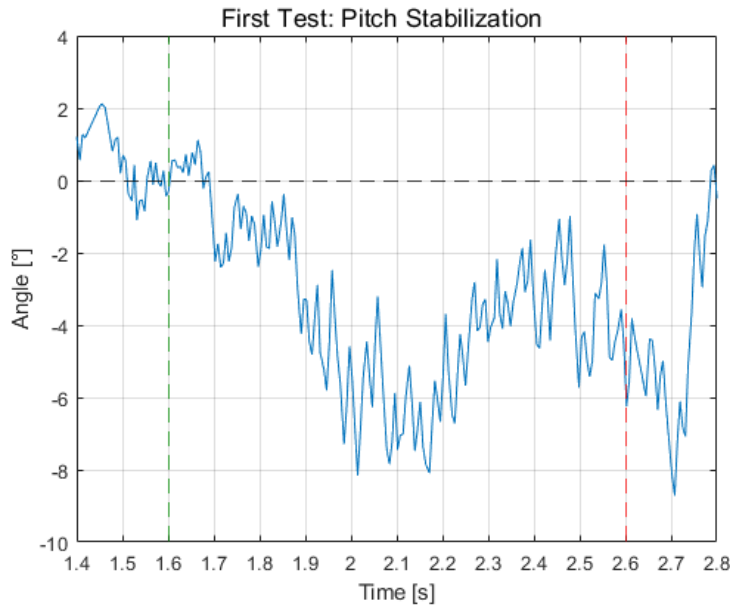


(b) Z-axis acceleration data with move mean.

Figure 22: Accelerometer data from the first test.



(a) Gyroscope data for roll.



(b) Gyroscope data for pitch.

Figure 23: Gyroscope data from the first test.

14.6 Third Test Graphs

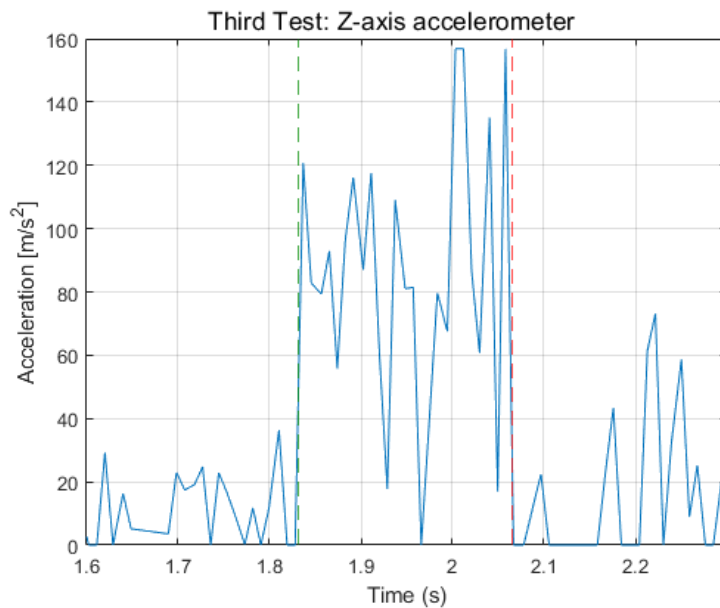
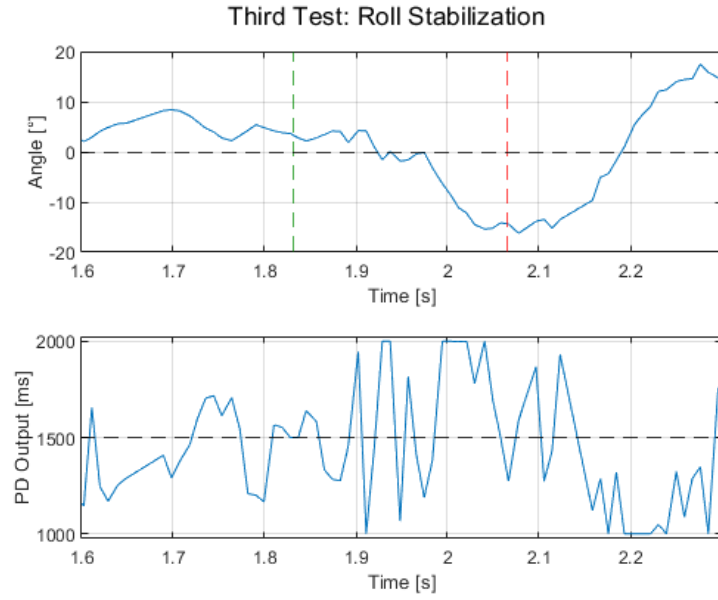
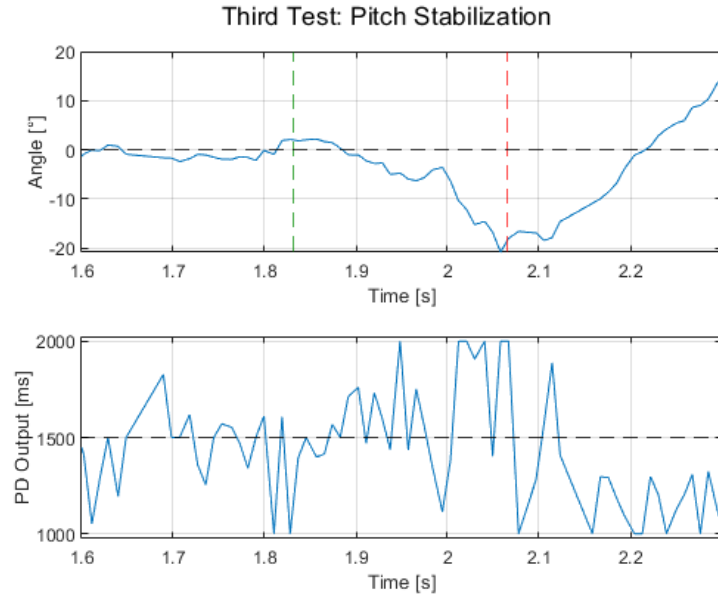


Figure 24: Z-axis acceleration data from the third test launch



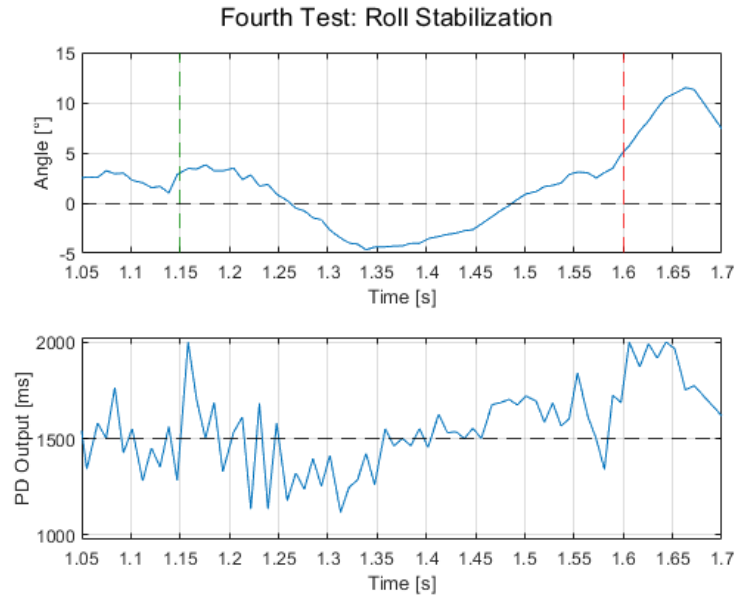
(a) Gyroscope data and PD controller output for roll.



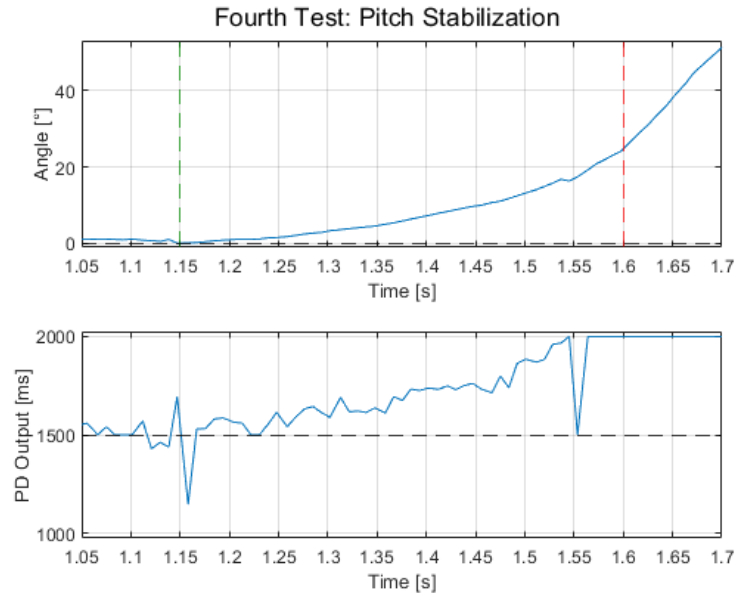
(b) Gyroscope data and PD controller output for pitch.

Figure 25: Gyroscope data and PD controller responses from the third test.

14.7 Fourth Test Graphs



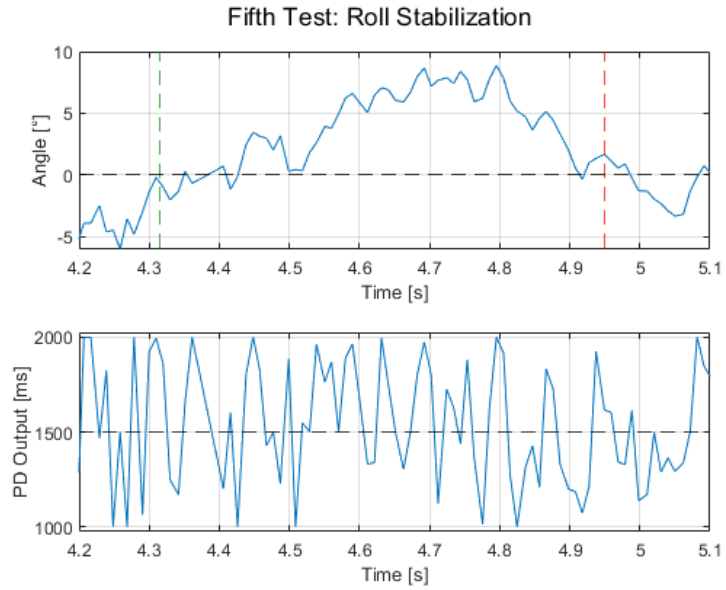
(a) Gyroscope data and PD controller output for roll.



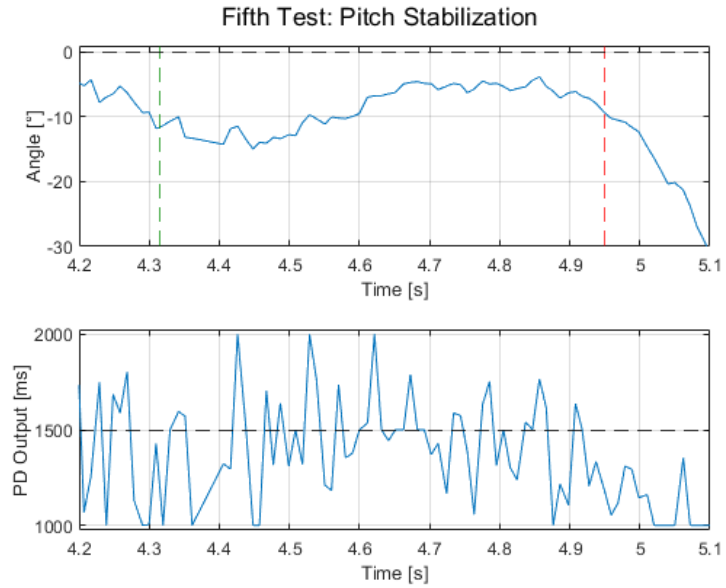
(b) Gyroscope data and PD controller output for pitch.

Figure 26: Gyroscope data and PD controller responses from the fourth test.

14.8 Fifth Test Graphs



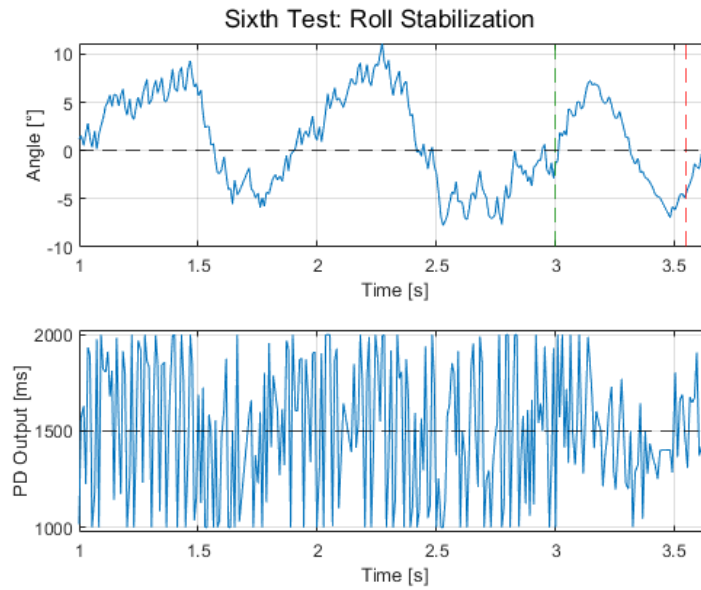
(a) Gyroscope data and PD controller output for roll.



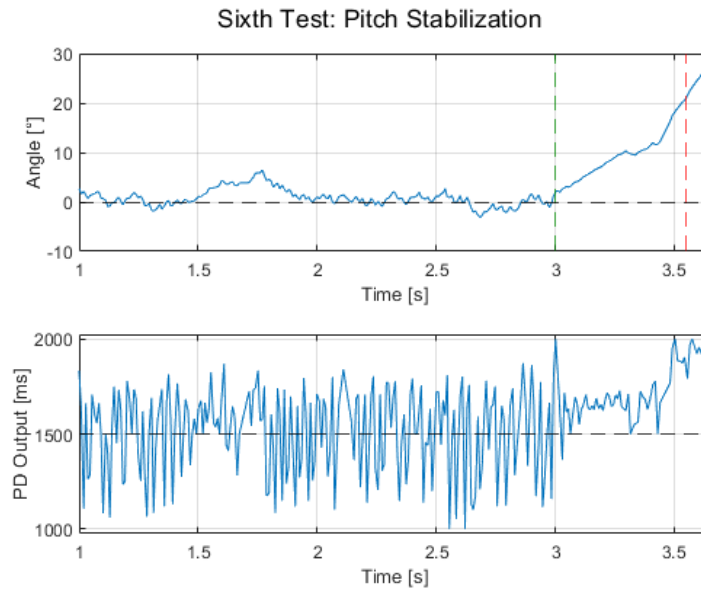
(b) Gyroscope data and PD controller output for pitch.

Figure 27: Gyroscope data and PD controller responses from the fifth test.

14.9 Sixth Test Graphs



(a) Gyroscope data and PD controller output for roll.



(b) Gyroscope data and PD controller output for pitch.

Figure 28: Gyroscope data and PD controller responses from the sixth test.